

AD-A260 240



2

ESL-TR-92-08

CRACK PATTERNS RESULTING FROM
HIGH STRAIN-RATE TESTS ON
CONCRETE

C. ALLEN ROSS

UNIVERSITY OF FLORIDA
GRADUATE ENGINEERING AND RESEARCH
CENTER
P.O. BOX 1918
EGLIN AFB, FL 32542-0918

MARCH 1992

FINAL REPORT

JANUARY 1991 - OCTOBER 1991

APPROVED FOR PUBLIC RELEASE:
DISTRIBUTION UNLIMITED

DTIC
SELECTED
FEB 17, 1993
S B



93-02984

2007



AIR FORCE ENGINEERING & SERVICES CENTER
ENGINEERING & SERVICES LABORATORY
TYNDALL AIR FORCE BASE, FLORIDA 32403

98 2 16 078

NOTICE

PLEASE DO NOT REQUEST COPIES OF THIS REPORT FROM
HQ AFESC/RD (ENGINEERING AND SERVICES LABORATORY).
ADDITIONAL COPIES MAY BE PURCHASED FROM:

NATIONAL TECHNICAL INFORMATION SERVICE
5285 PORT ROYAL ROAD
SPRINGFIELD, VIRGINIA 22161

FEDERAL GOVERNMENT AGENCIES AND THEIR CONTRACTORS
REGISTERED WITH DEFENSE TECHNICAL INFORMATION CENTER
SHOULD DIRECT REQUESTS FOR COPIES OF THIS REPORT TO:

DEFENSE TECHNICAL INFORMATION CENTER
CAMERON STATION
ALEXANDRIA, VIRGINIA 22314

| REPORT DOCUMENTATION PAGE | | | Form Approved OMB No. 0704-0188 | |
|---|---|--|---|--|
| <small>Public reporting burden for this collection of information is estimated to average 1 hour per response, including the time for reviewing instructions, searching existing data sources, gathering and maintaining the data needed, and completing and reviewing the collection of information. Send comments regarding this burden estimate or any other aspect of this collection of information, including suggestions for reducing this burden, to Washington Headquarters Services, Directorate for Information Operations and Reports, 1215 Jefferson Davis Highway, Suite 1204, Arlington, VA 22202-4302, and to the Office of Management and Budget, Paperwork Reduction Project (0704-0188), Washington, DC 20503.</small> | | | | |
| 1. AGENCY USE ONLY (Leave blank) | | 2. REPORT DATE March 1992 | 3. REPORT TYPE AND DATES COVERED Final Report 6 Jan 91-5 Oct 91 | |
| 4. TITLE AND SUBTITLE Crack Patterns Resulting From High Strain-Rate Tests on Concrete | | | 5. FUNDING NUMBERS C F08635-11-C-0111 | |
| 6. AUTHOR(S) C. Allen Ross | | | | |
| 7. PERFORMING ORGANIZATION NAME(S) AND ADDRESS(ES) University of Florida Graduate Engineering and Research Center P.O. Box 1918 Eglin AFB, FL 32542-0918 | | | 8. PERFORMING ORGANIZATION REPORT NUMBER | |
| 9. SPONSORING / MONITORING AGENCY NAME(S) AND ADDRESS(ES) Air Base Survivability Branch Engineering Research Division AF Civil Engineering Support Agency Tyndall AFB, FL 32403-6001 | | | 10. SPONSORING / MONITORING AGENCY REPORT NUMBER ESL TR 92-08 | |
| 11. SUPPLEMENTARY NOTES | | | | |
| 12a. DISTRIBUTION / AVAILABILITY STATEMENT Availability of this report is specified on reverse of front cover | | | 12b. DISTRIBUTION CODE | |
| 13. ABSTRACT (Maximum 200 words) <p>Surface crack patterns were obtained for compression of small concrete specimens at high strain rates in a Split-Hopkinson pressure bar (SHPB). Visible macrocracks were not discernible until the peak stress of the stress-strain curve. The peak stress and associated strain increase with increasing strain rate. Crack density (mm^2/mm^3) when plotted versus strain was found to increase very fast initially and then become asymptotic to a linear function of strain.</p> | | | | |
| 14. SUBJECT TERMS Split-Hopkinson Pressure Bar, High Strain Rate, Impulse Loading, Crack Density, Crack Pattern, Concrete Compression | | | 15. NUMBER OF PAGES 54 | |
| | | | 16. PRICE CODE | |
| 17. SECURITY CLASSIFICATION OF REPORT Unclassified | 18. SECURITY CLASSIFICATION OF THIS PAGE Unclassified | 19. SECURITY CLASSIFICATION OF ABSTRACT Unclassified | 20. LIMITATION OF ABSTRACT | |

EXECUTIVE SUMMARY

A. OBJECTIVE

The objective of this study was to observe and record real-time crack pattern and density associated with high-strain-rate compression tests of concrete.

B. BACKGROUND

Effects of increasing strain rate on concrete strength has been recognized and recorded for many years. Increases in compressive strength occurs very gradually up to an approximate critical strain rate of 100/sec. At this critical strain, abrupt changes in strength occur which show strain rate sensitivity orders of magnitude greater than at the lower strain rates. Other than the increase in strength and the associated strain with strain rate, the most discernible difference between the static and dynamic loadings in concrete are the changes in crack density, crack pattern, crack distribution and crack velocity. In quasi-static compressive tests on concrete, failure usually occurs by one or two major cracks running through the specimen resulting in two or three large fractured pieces. As the load or strain rate increases the crack pattern, density and distribution increase resulting in failure by multiple cracking and many smaller fractured pieces. The crack density is the basis for describing and defining a damage model for concrete.

C. SCOPE

The general approach in this study is to measure the crack density of concrete failure using a ultra-high-speed camera to photograph failure of small concrete specimens in a Split-Hopkinson pressure bar (SHPB).

D. METHODOLOGY

Ultra-high-speed-photography was used to observe concrete failure at strain rates of 50 to 300/sec. The resulting crack

patterns were enhanced using an image analysis system. Crack length per surface area was measured and correlated with strain at peak stress. A crack-density parameter was defined and compared with existing damage models.

E. TEST DESCRIPTION

High-strain-rate tests were conducted using the AF Civil Engineering Support Agency (AFCESA) SHPB on 50.8 mm diameter 50.8 mm long concrete specimens. Specimens were instrumented with crack initiation detectors (break circuits) and strain gages. Crack patterns were observed using a ultra-high-speed camera running at an equivalent rate of 100,000 frames per second.

F. RESULTS

Test results were obtained for eight different instrumented concrete specimens at eight different high strain rates. Other specimens were tested for crack patterns and crack distribution. No macrocracks were observed until the specimen reached the peak stress. Both peak stress and strain associated with peak stress increases with strain rate. Crack length per surface area of the specimen was found to be almost linear with strain. Real-time strain measurements show a static Poisson's ratio up to approximately 60 percent of the peak stress but approached 1.0 at time of peak stress. A damage parameter defined in terms of crack density of crack surface/volume was in good agreement with that predicted analytically.

G. CONCLUSIONS

The small concrete specimens tested in the AFCESA SHPB appear to fail by longitudinal macro cracking at the time of peak stress. The total crack length/unit surface area of the specimen starts at the strain associated with the peak stress, rises sharply and follows a linear function of strain rate up to a point of complete loss of load carrying capacity. A crack density parameter defined as a dimensionless ratio of crack volume/unit volume based on the

experimental data is in very good agreement with the quantity defined analytically. It has been shown that a damage parameter and related damage modulus may be obtained from experimental crack-density data.

DTIC QUALITY INSPECTED 3

| | |
|--------------------|--|
| Accession For | |
| NTIS GRA&I | <input checked="checked" type="checkbox"/> |
| DTIC TAB | <input type="checkbox"/> |
| Unannounced | <input type="checkbox"/> |
| Justification | |
| By | |
| Distribution/ | |
| Availability Codes | |
| Dist | Avail and/or Special |
| A-1 | |

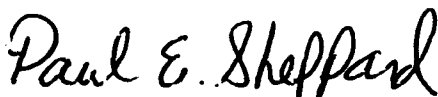
PREFACE

This report was prepared by the University of Florida Graduate Engineering and Research Center, Eglin AFB, Florida under contract No. F08635-91-C-0111 for the Air Base Survivability Branch, Engineering Research Division, Air Force Civil Engineering Support Agency, RACS/AFCEA Tyndall AFB, Florida 32403-6001.

This report summarizes the results of work to observe and measure crack density and distribution of concrete failure when tested at high strain rates. This work was initiated in January 1991 and completed in October 1991. Dr. C. Allen Ross served as principal investigator for the University of Florida. Capt. S.T. Kuennen and Mr. Paul Sheppard served as Project Officers for RACS/AFCEA.

This report has been reviewed by the Public Affairs Office and is releasable to the National Information Service (NTIS). At NTIS it will be available to the general public, including foreign nationals.

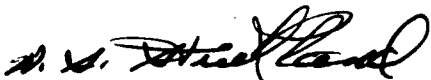
This report has been reviewed and is approved for publication.



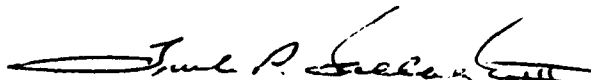
Paul E. Sheppard
Project Officer



Neil H. Fravel, Lt. Col, USAF
Chief, Engineering
Research Division



W. S. Strickland, GM-14
Chief, Air Base Survivability
Branch



Frank P. Gallagher, Col., USAF
Director, Civil Engineering
Laboratory

TABLE OF CONTENTS

| SECTION | TITLE | PAGE |
|---------|---|------|
| I | INTRODUCTION..... | 1 |
| | A. OBJECTIVE..... | 1 |
| | B. BACKGROUND..... | 1 |
| | C. SCOPE/APPROACH..... | 3 |
| II | EXPERIMENTAL TESTS..... | 5 |
| | A. TEST EQUIPMENT..... | 5 |
| | 1. Low-Strain-Rate Test Machine..... | 5 |
| | 2. Split-Hopkinson Pressure Bar (SHPB)..... | 6 |
| | 3. Image Converter Camera..... | 8 |
| | 4. Image Analysis System..... | 8 |
| | 5. Transient Data Recorder (TDR)..... | 9 |
| | B. TEST PROCEDURE..... | 9 |
| | 1. Specimen Preparation..... | 9 |
| | 2. Test Setup and Procedure..... | 11 |
| | 3. Sample Raw Data..... | 14 |
| III | DAMAGE MODEL..... | 19 |
| | A. INTRODUCTION..... | 19 |
| | B. APPLICATION..... | 22 |

TABLE OF CONTENTS (CONCLUDED)

| | | |
|----|--|----|
| IV | RESULTS AND DISCUSSION..... | 23 |
| | A. HIGH-STRAIN-RATE CONCRETE DATA..... | 23 |
| | B. CRACK INITIATION AND DENSITY..... | 28 |
| | 1. Crack Initiation..... | 28 |
| | 2. Crack Density and Damage Model..... | 28 |
| | C. DISCUSSION..... | 33 |
| | 1. Crack Initiation and Strain Data..... | 33 |
| | 2. Crack Density and Damage Model..... | 42 |
| V | CONCLUSIONS AND RECOMMENDATIONS..... | 47 |
| | REFERENCES..... | 48 |

LIST OF FIGURES

| FIGURE | TITLE | PAGE |
|--------|--|------|
| 1 | Comparison of Strain-Rate Sensitivity for Compression, Flexure and Tension..... | 2 |
| 2 | Schematic of a Compressive Split-Hopkinson Pressure Bar.. | 7 |
| 3 | Schematic of Instrumented Specimen with Break Circuits (BC) and Strain Gages (SG)..... | 10 |
| 4 | Schematic of White Painted Surface on Specimen and Camera Position | 12 |
| 5 | General Test Setup for Instrumented Test Specimen..... | 13 |
| 6 | Copy of Raw Film data Taken from the High-Speed Camera and Strain Traces of the Incident, Reflected and Transmission Pulses..... | 17 |
| 7 | Compressive and Tensile Strength as a Function of Strain Rate Collected at RACS/AFCESA..... | 21 |
| 8 | Damaged Poisson's Ratio Versus Crack Density for Various Values of Undamaged Poisson's Ratio..... | 25 |
| 9 | Compressive Concrete Data Obtained Using the RACS/AFCESA SHPB..... | 27 |
| 10 | Strain-Rate Effects on the Shape of the Stress-Strain Curve..... | 28 |
| 11 | Strain-Rate Effects on the Strain at Peak Stress..... | 29 |
| 12 | Tensile Concrete Data Obtained Using the RACS/AFCESA SHPB..... | 30 |
| 13 | Break Circuit Traces for the Array on the Incident End of the Specimen. (Array A of Figure 3, Specimen DCI-2, Strain rate = 92/sec)..... | 32 |
| 14 | Break Circuit Traces for the Array at Midsection of the Specimen (Array B of Figure 3, Specimen DCI-2, B Strain Rate = 92/sec)..... | 33 |
| 15 | Break Circuit Traces for the Array on the Transmitter End of the Specimen (Array C of Figure 3, Specimen DCI-2, Strain rate = 92/sec)..... | 34 |

LIST OF FIGURES (CONCLUDED)

| FIGURE | TITLE | PAGE |
|--------|---|------|
| 16 | Strain Gage Traces for Specimen DCI-2, Strain Rate = 92/sec..... | 32 |
| 17 | Crack Patterns for Deforming Specimen DCI-2, Strain Rate = 92/sec. Ten Microseconds Between Frames... | 34 |
| 18 | Crack Patterns for Deforming Specimen DCI-9, Strain Rate = 65/sec. Ten Microseconds Between Frames... | 35 |
| 19 | Crack Patterns for Deforming Specimen DCI-8, Strain Rate = 22/sec. Ten Microseconds Between Frames... | 36 |
| 20 | Stress and Strain Versus Time after Trigger for Specimen DCI-2. This Data Obtained from SHPB Traces..... | 37 |
| 21 | Crack Surface/Volume Versus Compressive Axial Strain for Different Strain Rates..... | 38 |
| 22 | All Crack Surface/Volume Data Excluding Initial Strains Used in Linear Regression..... | 39 |
| 23 | Stress-Strain Curve for Specimen DCI-2, Strain Rate = 92/sec. Range of Strain 0.0 to 1.0%..... | 40 |
| 24 | Stress-Strain Curve for Specimen DCI-2, Strain Rate = 92/sec. Range of Strain 0.0 to 3.0%..... | 41 |
| 25 | Transverse/Axial Strain Ratio for Specimen DCI-2, Strain Rate = 92/sec..... | 43 |

SECTION I INTRODUCTION

A. OBJECTIVE

The major objective of this study was to observe and record real time crack pattern density associated with high-strain-rate compression tests of concrete.

B. BACKGROUND

The effect of increasing strain rate on concrete strength has been recognized for many years. Recent concrete research data for compression tests are reported in References 1 and 2, tensile data in References 2 and 3 and flexural data are reported in reference 4. Plots of strength ratios (dynamic/static strength) verses logarithm (base 10) of strain rate show rather-moderate increases in the strength ratios beginning at strain rates as low as 10^{-7} to 10^{-8} /sec. A schematic of this is shown in Figure 1. Rather abrupt changes in the strength ratios for the three modes of loading occur at higher strain rates but these abrupt changes or increased strain-rate sensitivity occur at different strain rates for the three different loadings. This is shown schematically for compression, tension and flexure in Figure 1.

Other than the increase in concrete strength with increasing strain rate, probably the most discernible difference between the static and dynamic loading are the changes in the crack pattern, crack density, crack distribution, and crack velocity. In quasi-static compressive tests on concrete, failure usually occurs by one or two major cracks running through the specimen resulting in two or three fractured pieces. As the load or strain rate increases

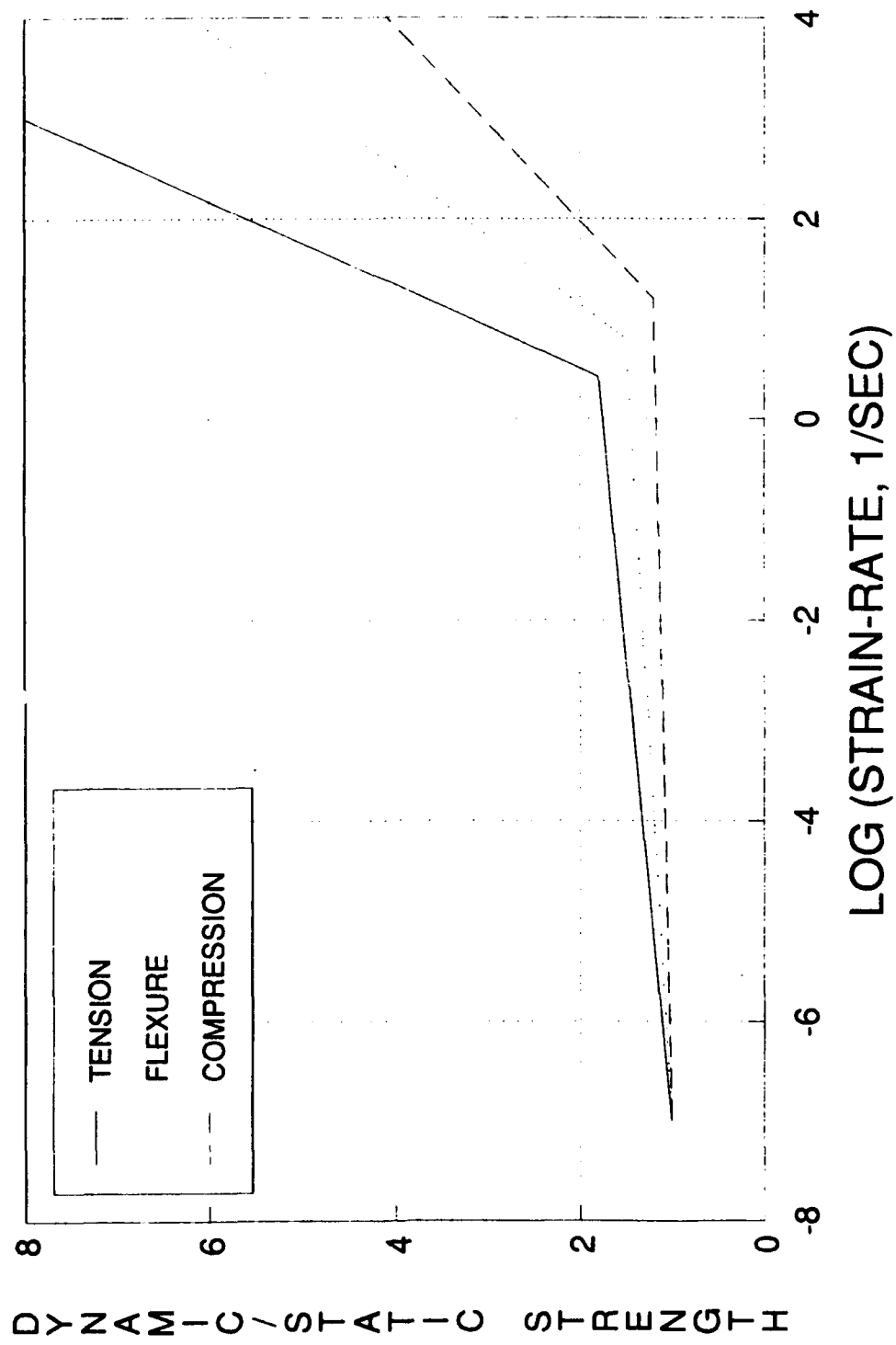


Figure 1. Comparison of Strain-Rate Sensitivity of Compression, Flexure and Tension.

the crack density increases and failure occurs by multiple cracking with many smaller fractured pieces. At the high load-rate, a larger number of cracks are present with much more uniformity, and the specimen is reduced to rubble.

A discussion of the many models currently employed in analysis of concrete material and concrete structures is beyond the scope of this paper. However, it appears that continuum models are much easier to use and install in the many numerical finite-element and finite-difference computer models currently in use today. For this reason, a continuum damage model to be discussed later, is presented as one way of determining load carrying ability and describing the extent of damage in concrete material and structures. Additionally, this damage model uses as its basis, the experimentally determined material properties currently being produced at the Air Base Survivability Branch, Air Force Civil Engineering Support Agency (RACS/AFCESA).

C. SCOPE/APPROACH

The general approach in this study will be to measure the crack distribution resulting from high-strain-rate compression of concrete specimens. This will be accomplished in real time using the Split-Hopkinson pressure bar (SHPB) and related equipment located at RACS/AFCESA. This system will allow simultaneous recording of dynamic failure mechanisms, crack patterns, stress, strain and strain rate, all in real time. Crack pattern and distribution will be determined using the ultra-high-speed image converter camera coupled with an image analysis system for crack high-lighting and measuring crack length.

SECTION II

EXPERIMENTAL TESTS

A. TEST EQUIPMENT

1. Low-Strain-Rate Test Machine

Initial testing was accomplished on an MTS® 880 (MTS Systems Corp., Minneapolis, Minnesota) closed-loop machine with a 50,000 pound capacity. Special tension platens are also available for cementing concrete tensile specimens. In addition, 1-inch (2.54 cm) gage length clip-on strain gages are available in the strain range associated with concrete. The difficulty in using this machine and the clip-on gages is that, when concrete cracking starts, the clip-on gages become inoperative and no record of the strain beyond the initial cracking stage is available. If only the elastic portion of the stress-strain curve and the peak stress are of interest then this method is sufficient. However, since the softening portion or stress-strain beyond the peak stress was of interest another method of low-strain-rate testing was pursued.

The second method consisted of a Forney® System 2000 (Forney, Inc., Wampum, PA.) material test machine with 400,000 pound capacity, a Sensotec® Model 34, 400,000-pound load cell placed in series with the specimen and two Sensotec® (Sensotec Inc., Columbus, OH) Model S2C-100 linear voltage differential transducers (LVDT) to measure the relative displacement between the platens. This system, when run in a displacement control mode, produces the relative platen displacement along with the load on the softening side or negative slope of the load-displacement curve. This system was used to give three strain rates from 10^{-1} /sec. to 10^{-3} /sec.

2. Split-Hopkinson Pressure Bar (SHPB)

A 2 inch diameter Split-Hopkinson Pressure Bar (SHPB) located in RACS/AFCEA was used for the high-strain-rate tests. This SHPB system is described in detail in Reference 2. Compression tests on concrete from a strain rate of approximately 1/sec up to 500/sec have been conducted using this system. The SHPB system is composed of three major components, a bar assembly, a data acquisition system and data analysis system.

The bar assembly consist of an incident or input bar, a transmitter or output bar, a striker bar, a striker bar launching barrel and gas gun. A schematic of the overall SHPB system is shown in Figure 2.

In the compression mode, the striker bar impacts the incident bar setting up a stress wave whose magnitude and length are proportional to the velocity and striker bar length, respectively. The incident wave impinges on the specimen and part of the wave is reflected back into the incident bar and part of the wave is transmitted into the transmitter bar. It can be shown [2] that, for a specimen whose length is small compared to the length of the stress pulse, the integral of the reflected pulse is proportional to the strain in the specimen and the transmitted pulse is proportional to the stress in the specimen. The incident and reflected pulses are recorded from the incident bar strain gage.

The strains associated with the three pulses are monitored by a full bridge of strain gages located on each bar, equidistant from the specimen. The strain signals are partially amplified and conditioned using a model 2311 Strain Gage Conditioning Amplifier (Measurements Group, Inc., Raleigh, NC). After conditioning, the strain signals are recorded and stored on a 4094 Nicolet® digital oscilloscope (Nicolet Instrument Corp.,

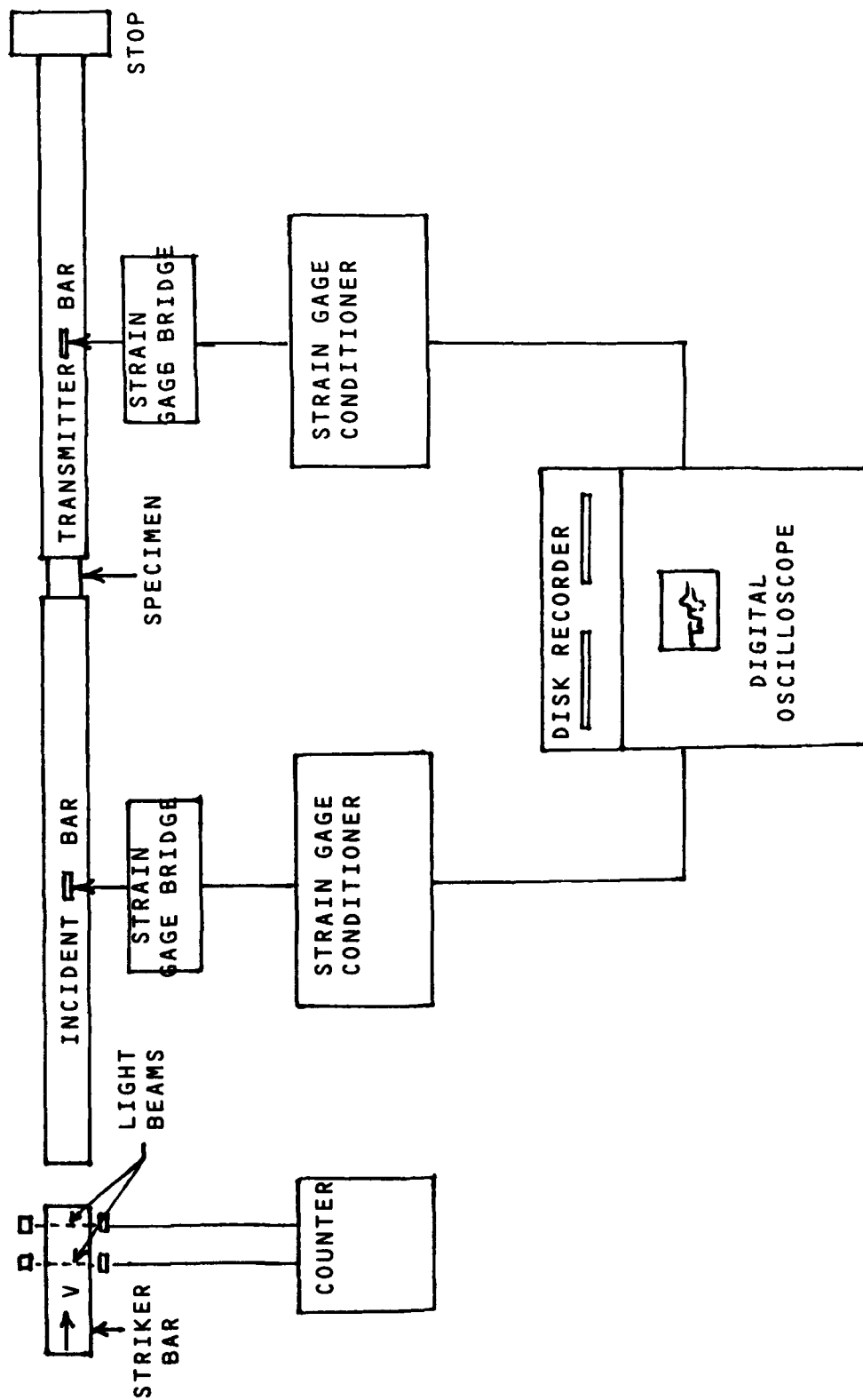


Figure 2. Schematic of a Compressive-Split-Hopkinson Pressure Bar.

Madison, WI). The signals are then stored on floppy disks for permanent storage and further analysis.

Stress-strain, stress-time, strain-time and strain rate time curves are generated using an IBM® 280C AT personal computer with VU-POINT® and LOTUS® software. A dispersion correction program [5] is used to correct the signals for dispersion, correct for phase change from the strain gage to the specimen and convert the signals to stress, strain and strain rate.

3. Image Converter Camera

Crack patterns of fracturing concrete compression specimen were observed using a IMACON® 790 ultra-high-speed camera (Hadland Photonics, Inc., Cupertino, CA) running at an equivalent framing rate of 100,000 frames/sec. This system and framing rate produces eight to sixteen frames on a 4 inch X 3.35 inch, 3000 ASA Polaroid film with 10 microseconds between frames. Other equivalent framing rates up to a million frames/sec are available but were not used. Synchronization between the camera and the event was handled by a multiple-delay generator and high intensity flash unit were used for lighting. The delay generator and flash unit were obtained as part of the camera system.

4. Image Analysis System

A Buehler® Omnimet® II Image Analysis System (Buehler Inc., Lake Bluff, IL) was used to enhance the crack pattern obtained from the SHPB tests. This system has multifaceted capability for image analysis but for this study only the electronic "paint" mode was used to enhance the cracks, an area-measurment option was used to measure the total crack length and the enhanced image was stored as a grey image.

5. Transit Data Recorder (TDR)

For the instrumented direct-compression specimens, 19 sets of data were recorded. For these special tests, a Pacific® Model 5775 Master Transit Data Recorder (TDR) was used to record sixteen channels of this data. These data may be down-loaded into a special format for display in the LOTUS® software for plotting.

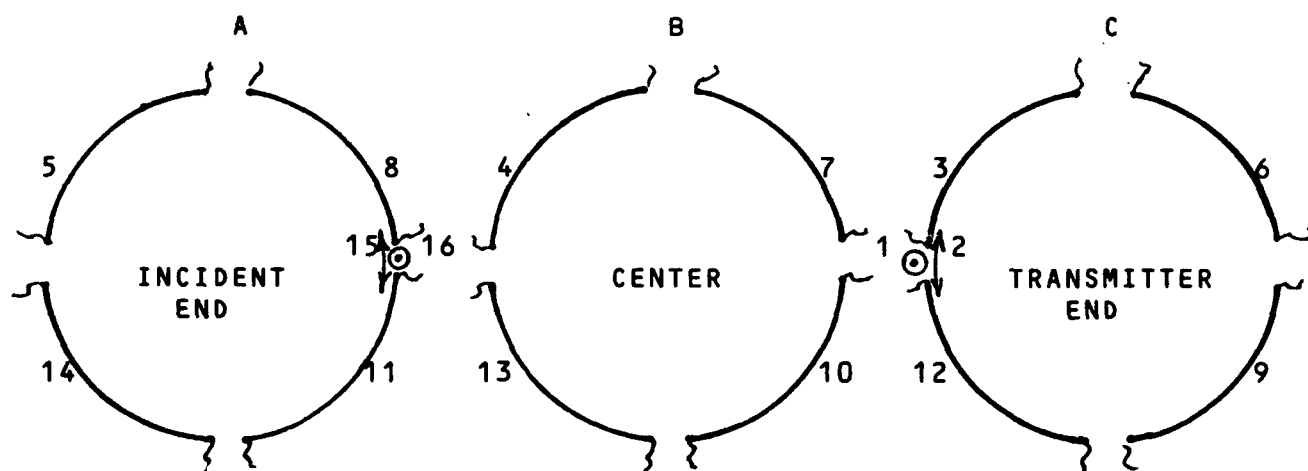
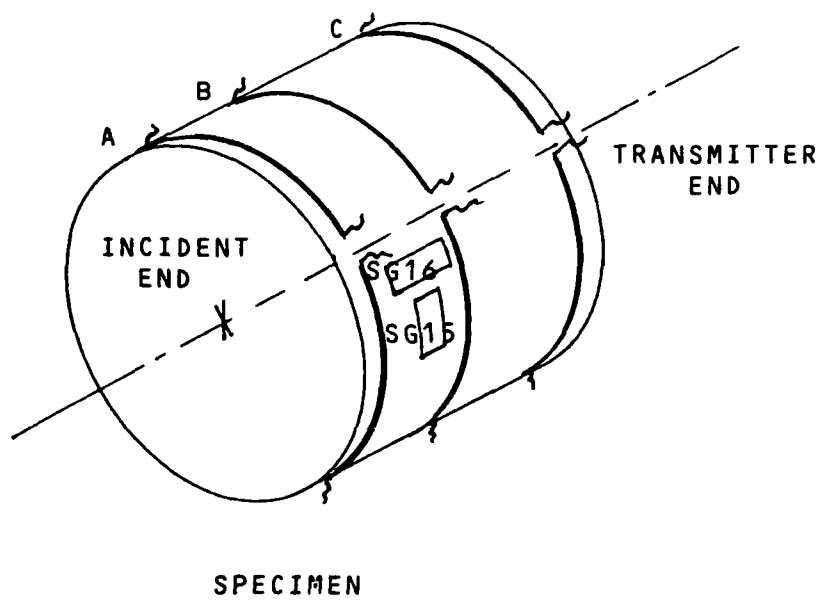
B. Test Procedure

1. Specimen Preparation

The concrete specimens were cast in two 12 inch X 12 inch X 6 inch (30.5 X 30.5 X 15.2 cm) boxes, allowed to set up for 24 hours and placed in water. Specimens were cored under water and cut to length using a water spray at approximately 28 days, then placed back in water for an additional 32 days. At the end of the 60-day water bath the specimens were placed on paper towels and allowed to dry 20 days in normal air-conditioning before testing. The concrete mix proportions are given in Table 1. The wet 7-day strength was 5,000 psi (34.48 MPa) and the strength after the 20-day dry period was 7,000 psi (48.28 MPa). The final specimen size was 2.00 ± 0.010 inch diameter, 2.00 ± 0.005 inch long (5.080 ± 0.025 cm diameter X 5.080 ± 0.013 cm long).

TABLE 1. CONCRETE MIX PROPORTIONS

| COMPONENT | AMOUNT | |
|--------------------------------------|--------|----------|
| Course Aggregate 0.38 in. (0.97 cm.) | 62.5 | (28.38) |
| Fine Aggregate (ASTM C33) | 50.0 | (22.70) |
| Portland Cement | 25.0 | (11.35) |
| "F" Fly Ash | 01.8 | (0.82) |
| Deairing Agent | 00.045 | (0.021) |
| Water | 15.0 | (6.81) |



BREAK CIRCUITS(BC) AND STRAIN GAGE(SG)
LOCATIONS

Figure 3. Schematic of Instrumented Specimen with Break Circuits (BC) and Strain Gages (SG).

Both instrumented and uninstrumented specimens were tested at high strain rates in the SHPB. For the instrumented specimens the general idea was to try to determine when fracture or cracking actually began relative to the stress-strain response. Ten concrete test specimens were instrumented as shown in Figure 3. The break circuits (BC) were formed by painting four brittle electrical conducting lines each approximately 90° around the circumference of the specimen at each end and mid-length of the specimen. These lines were painted approximately 1.0 to 1.5 mm wide using Nickel Print (CG Electronics, Rockford, IL), a fast drying liquid matrix containing metallic particles, normally used for repair of circuit boards. At each end of the 90° arc a small diameter wire conductor was cemented to the specimen with a short length of each wire conductor painted as part of the BC. The BC was then placed in parallel with a resistor and in series with nine volts DC. When the BC is broken an abrupt voltage jump is registered on the recording device.

Several methods of enhancing the cracks formed during the test were tried. The most successful method was to paint the specimen with a white shoe polish. Several white spray paints were used but were unsatisfactory, as all had some electrical conductance which shorted the break circuits. It was determined experimentally that the 50 mm lens of the high speed camera had sufficient depth-of-field to cover a 60° arc on the 2.0 inch (50.4 mm) diameter specimen. This means that only one-sixth of the specimen area could be photographed during the test. This arrangement is shown schematically in Figure 4.

2. Test Setup and Procedure

The overall test setup is shown in Figure 5. Operation of the SHPB is given in detail in Reference 2, but basically, the

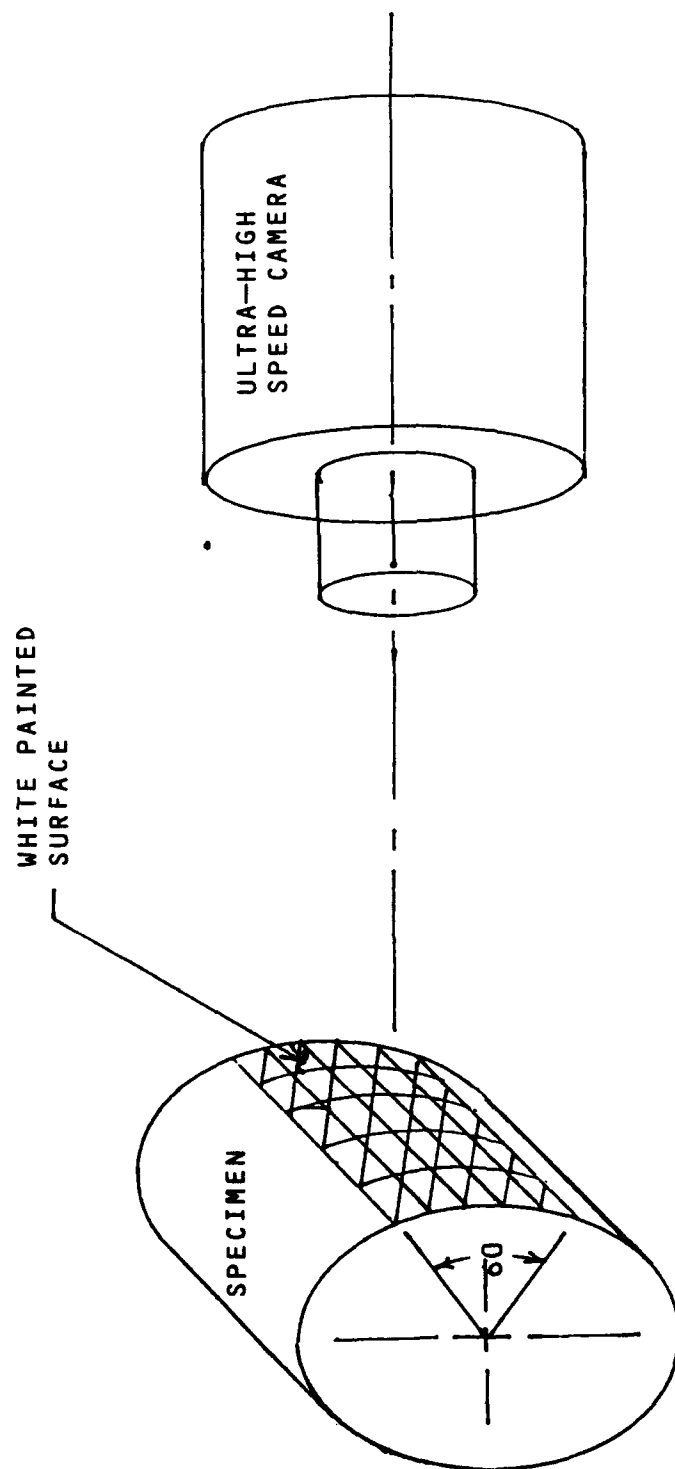


Figure 4. Schematic of White Painted Surface on Specimen and Camera Position.

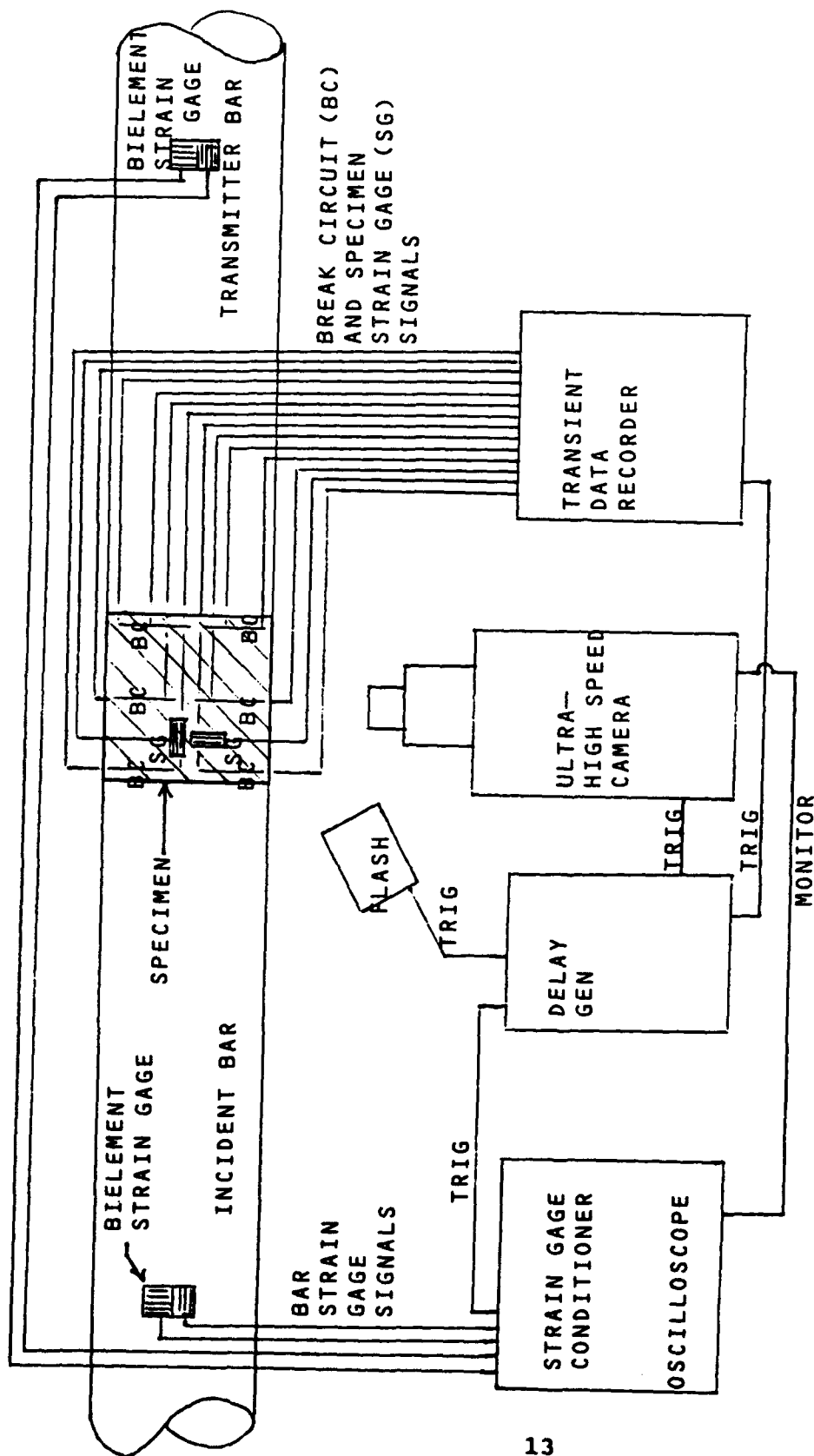


Figure 5. General Test Setup for Instrumented Test Specimen.

striker bar is put in motion by dumping high pressure nitrogen from the gas gun into the barrel containing the striker bar. The striker bar/incident bar impact generates the incident stress wave which when crossing the incident bar strain gage gives the initial trigger signal for the oscilloscope. Care must be taken to set the proper amplification of the strain-gage conditioner to give at least a negative one volt output to trigger the first delay of the delay generator. The output of the incident gage channel of the strain gage conditioner is fed simultaneously to the oscilloscope and the delay generator. All channels of the oscilloscope are triggered from this one channel. The time of trigger for the delay generator can be determined by recording the time of negative one volt from the incident gage signal recorded on the oscilloscope. Both the incident strain signal and the reflected signal are recorded on the same channel and the transmitted strain signal is recorded on a different channel. As a check on the delay generator the camera monitor signal is also recorded on the oscilloscope. This camera monitor signal also serves as a check on the interframe delay of the camera.

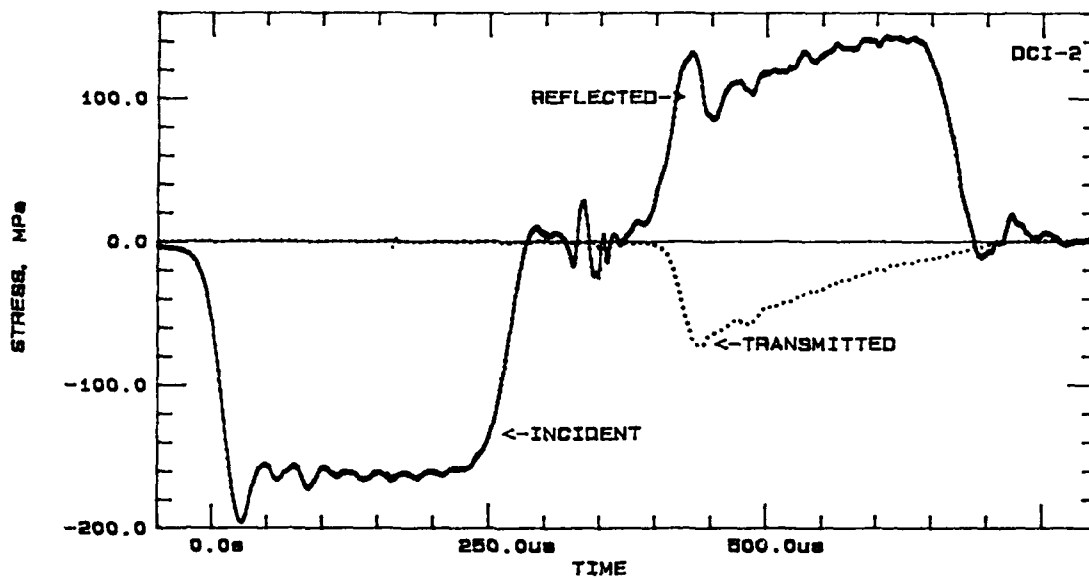
Upon determining the delay required for the camera the first delay channel is set for the camera delay time less 60 microseconds. The second delay which triggers the camera is set for 60 microseconds, the time required for the flash unit to reach peak intensity. In addition to the flash units the first delay generator also triggers the transit data recorder (TDR). The high speed camera is shuttered by hand just prior to the event. The small amount of light entering prior to the flash unit sequence has no effect on the film.

3. Sample Raw Data

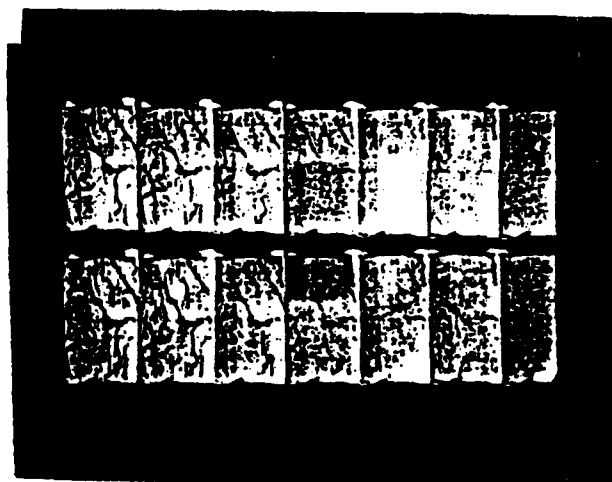
As indicated above the oscilloscope records the incident, reflected and transmitted pulses. A sample of this raw data is shown in Figure 6a. This data is stored on floppy disks to be used

in the computer program for phase correction, dispersion correction and files for plotting of stress, strain and strain rate.

Film taken directly from the camera is difficult to read without magnification and is difficult to copy as shown in Figure 6b. The image analysis system is used to enhance the data and transfer to the computer for reproduction.



(a) Strain-Gage Traces



(b) High-Speed Film

Figure 6. Copy of Raw Film Data Taken from the Gigh-Speed Camera and Strain Traces of the Incident, Reflected and Transmitted Pulses.

SECTION III DAMAGE MODEL

A. INTRODUCTION

Continuum damage models [6] introduce internal state variables into the analysis which represent on a macroscopic scale, the distribution of microcracks in the material. The model discussed here is written in terms of a single damage parameter which combines the theory of fracture mechanics and a statistical treatment to account for the random distribution of the microcracks.

The crack-density parameter, to be introduced in the next section, is based on a distribution of flaws per unit volume that are active at a given mean stress and the characteristic length cubed of the nominal fragment size obtained at a given mean stress and strain rate. Even though it can be based upon microcracks in theory, the visible macrocrack distribution may be related to tensile strength and fracture toughness of brittle materials. Since the crack density parameter is proportional to a characteristic length cubed, the macrocracks have the major influence on the parameter. The unknowns are the number of active flaws and proportionality constant between fragment size cubed and crack density. These unknowns get absorbed mathematically into material constants that can be determined experimentally.

A crack density parameter C_d , defined as the volume fraction of voids, may be used to describe an effective bulk modulus K of the damaged or cracked solid. This relationship is given as [7],

$$\frac{\bar{K}}{K} = 1 - \frac{16}{9} \frac{(1-\bar{\nu}^2)}{(1-2\bar{\nu})} C_d \quad (1)$$

where K and ν are bulk modulus and Poisson's ratio of the undamaged material and $\bar{\nu}$ is the Poisson's ratio of the damaged material. Rewriting Equation (1) as

$$\bar{K} = K(1-D) \quad (2)$$

where D is the 2nd term on the RHS of Equation 1, defined as a damage factor [7] and written as

$$D = \frac{16}{9} \frac{(1-\bar{\nu}^2)}{(1-2\bar{\nu})} C_d. \quad (3)$$

D ranges from 0 to 1.0 and in turn \bar{K} varies in the inverse manner. At $\bar{K} = 0$ the material has lost all of its ability to support a load. It is shown in Reference 8 that the damage factor D may be written as

$$D = \left(\frac{40}{9} \frac{K_{IC}^2}{\rho c} \right) \frac{k \epsilon^m}{\dot{\epsilon}^2} \quad (4)$$

where K_{IC} is the fracture toughness for Mode I fracture, ρ is the density, c is the one dimensional wave speed $(E/\rho)^{1/2}$, E is Young's modulus, ϵ , $\dot{\epsilon}$ are strain and strain rate respectively and k , m are material constants obtained experimentally. K_{IC} is a fracture mechanics parameter and material property which may vary with strain rate while, k and m are determined from high strain-rate data. Although the model discussed above is based on tensile stress it could very well apply to compressive data where the crack density is associated with a transverse tensile strain in a axial compression specimen. Both compressive and tensile high strain-rate data has been generated using the RACS/AFCEA SHPB. A collection of this data is shown in Figure 7. Both k and m may be determined for both compression and tension from data shown in Figure 7.

STRAIN RATE EFFECTS ON CONCRETE STRENGTH

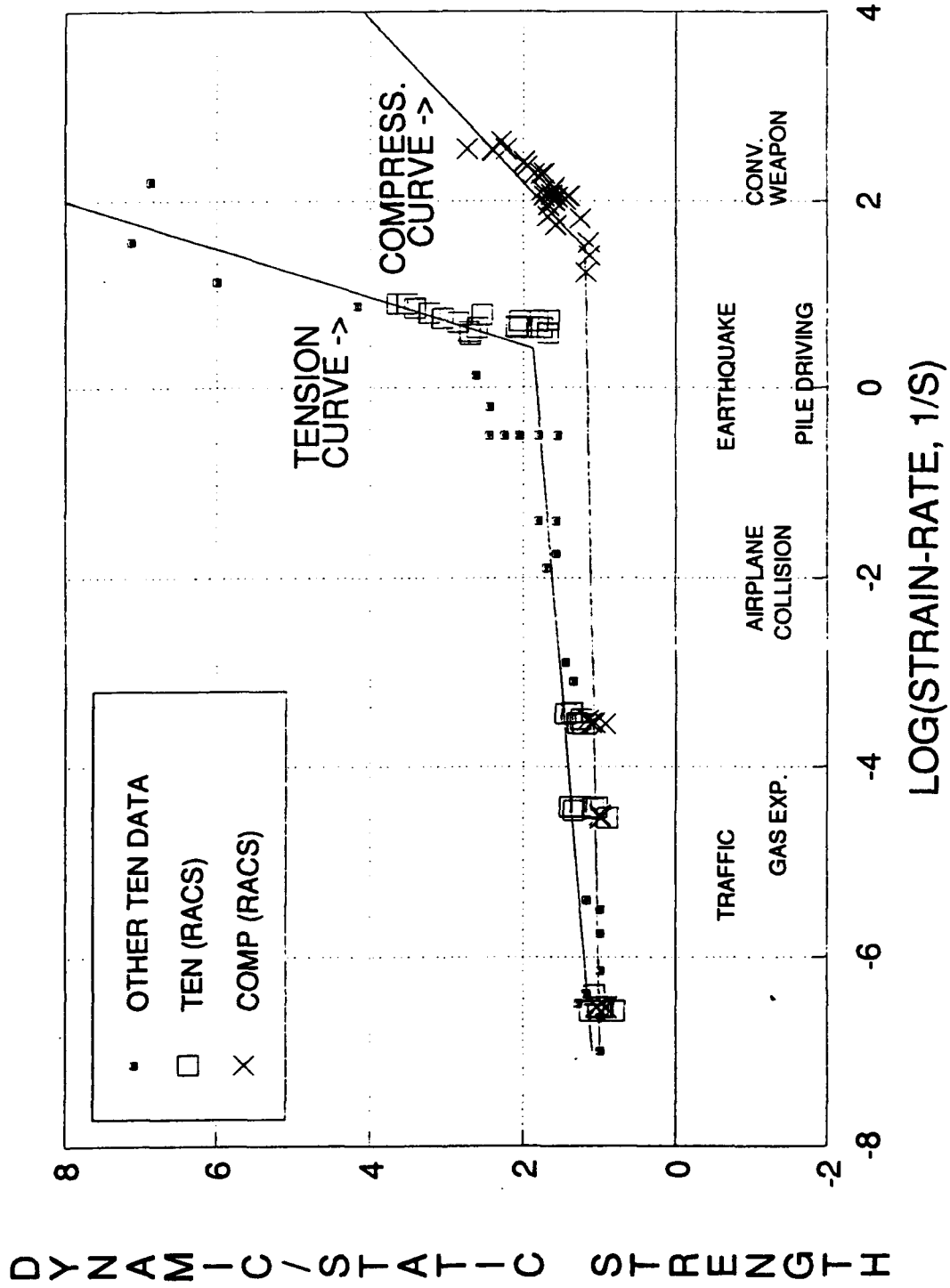


Figure 7. Compressive and Tensile Strength as a Function of Strain Rate Collected at RACS/AFCEA

It is shown in Reference 8,

$$\log f'_i = \frac{2}{m} \log \dot{\epsilon} + C_0 \quad (5)$$

where f'_i is tensile strength and C_0 is the intercept of the $\log f'_i$ - $\log \dot{\epsilon}$ plot. This expression gives m as twice the inverse of the slope of the $\log f'_i$ - $\log \dot{\epsilon}$ curve and the term k of Equation (4) may then be determined from the expression

$$\log k = m \left[\log \frac{3Km}{f'_i} - \frac{m+1}{m} \log(m+1) \right] - \log \left[\frac{40}{9} \frac{K_{IC}^2}{\rho c \dot{\epsilon}^2} \right] \quad (6)$$

B. APPLICATION

From references [7] and [8] it is shown that C_d may be written in terms of the damaged and undamaged Poisson's ratios, ν and $\bar{\nu}$. If C_d is known experimentally then $\bar{\nu}$ and D may be calculated without the use of k and m . This appears advantageous since the value of k is on the order of 1.0×10^{22} to 1.0×10^{23} and is not nearly as accurate at the m term.

Rewriting Equation (3) as

$$D = (16/9) f_1(\bar{\nu}) C_d \quad (7)$$

where

$$f_1(\bar{\nu}) = (1 - \bar{\nu}^2) / (1 - 2\bar{\nu}), \quad (8)$$

gives the damage function in terms of only two unknowns. A rather complicated expression of crack density C_d in terms of ν and $\bar{\nu}$ is given in [7,8] but by neglecting higher order terms it may be reduced to give the damaged Poisson's ratio $\bar{\nu}$ in terms of crack density C_d and Poisson's ratio ν ,

$$\bar{\nu} = \nu [1 - (16/9) C_d] \quad (9)$$

Using Equations (7,8,9) the damage function D may be calculated from an experimentally determined crack density C_d .

Remembering C_d is a volume fraction of voids and dimensionless then it varies from 0.0 to 1.0. Upon examination of Equation (9) the damaged Poisson's ratio $\bar{\nu}$ is equal to ν when $C_d = 0.0$ and equal to 0.0 when $C_d = 9/16$. Using these and observing that $\bar{\nu}$ is linear with C_d from Equation (9), a plot of $\bar{\nu}$ versus C_d for various values of ν is given in Figure 8.

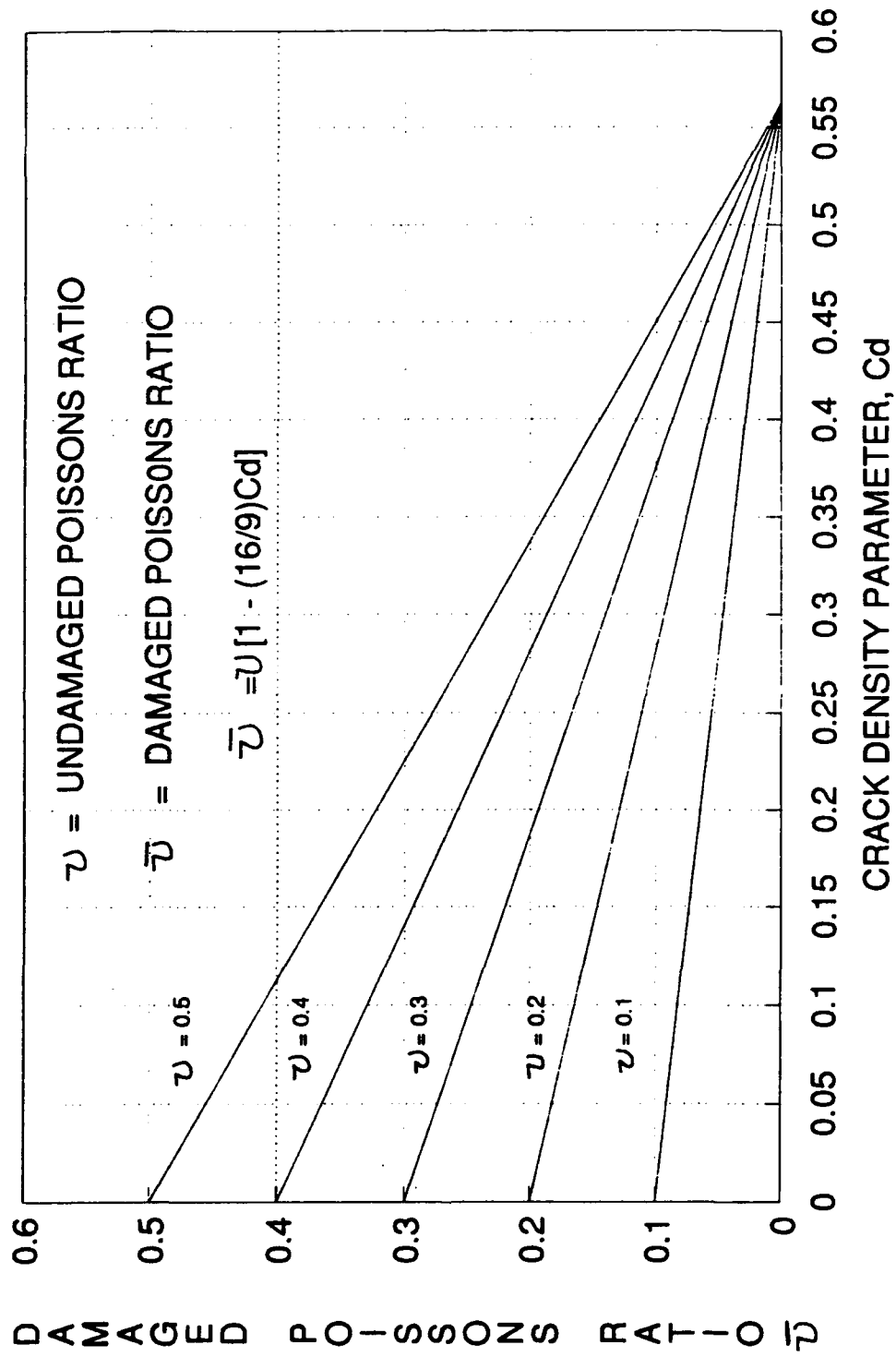


Figure 8. Damaged Poisson's Ratio Versus Crack Density for Various Values of Undamaged Poisson's Ratio.

SECTION IV

RESULTS AND DISCUSSION

A. HIGH-STRAIN-RATE CONCRETE DATA.

Strain-rate effects on concrete compressive strength has been examined experimentally by many investigators but more recent data may be found in References (1,2,9 and 10). In addition considerable concrete compressive strength data was generated in completion of this study. These data, along with other previous data obtained using the RACS/AFCEA SHPB, are shown in Figure 9. The strain-rate effects on compressive strength are fairly moderate up to a critical strain rate of approximately 50 to 100/sec. Above this critical strain rate, a rather high-rate sensitivity occurs. The increase in the compressive strength is also accompanied by an increase in the strain at peak stress. This is shown in Figure 10, which presents stress-strain curves with various strain rates. This means that both peak stress (strength) and strain associated with the peak stress are functions of strain rate.

In an effort to quantify the effect of strain rate on the strain at peak stress, the compressive data on file was reviewed. Results of this review are shown in Figure 11. Here the strain is plotted versus strain rate rather than the logarithm as in the previous figures. It does not appear that normalizing the data or plotting it against the log (strain rate) would be of any benefit as large scatter is present in the data.

Strain-rate effects in tension are similar to that in compression except that the higher rate sensitivity occurs at a lower strain rate than that of compression. The critical strain rate in tension is on the order of 1.0 to 10/sec and is shown in Figure 12. It is also observed that the slope of the high-rate sensitivity curve of the tensile data is slightly larger than that

STRAIN-RATE EFFECTS ON CONCRETE STRENGTH COMPRESSION TESTS

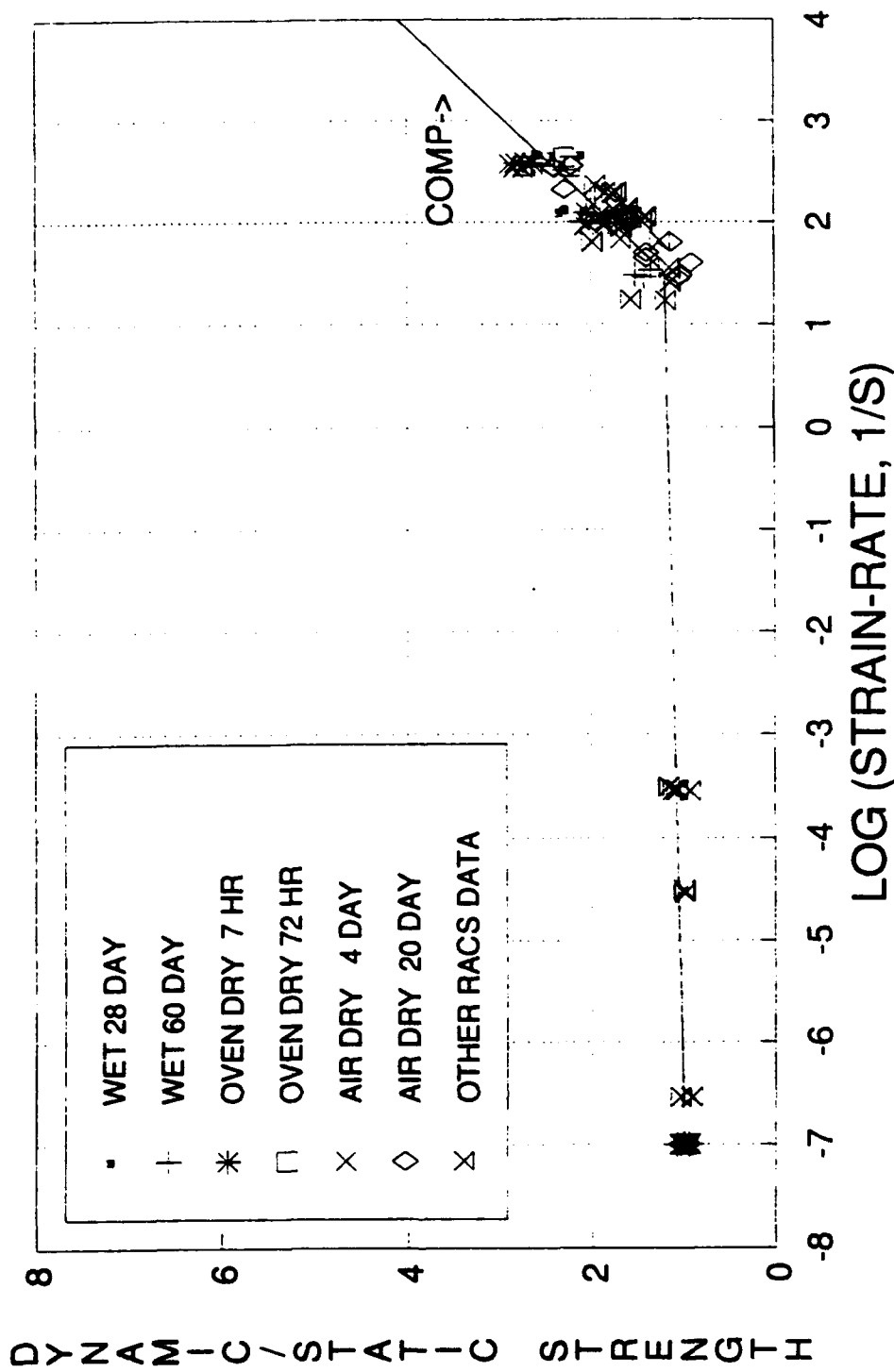


Figure 9. Compressive Concrete Data Obtained Using the RACS/AFCEA SHPB.

STRAIN RATE EFFECTS ON CONCRETE

SHPB COMPRESSION TESTS

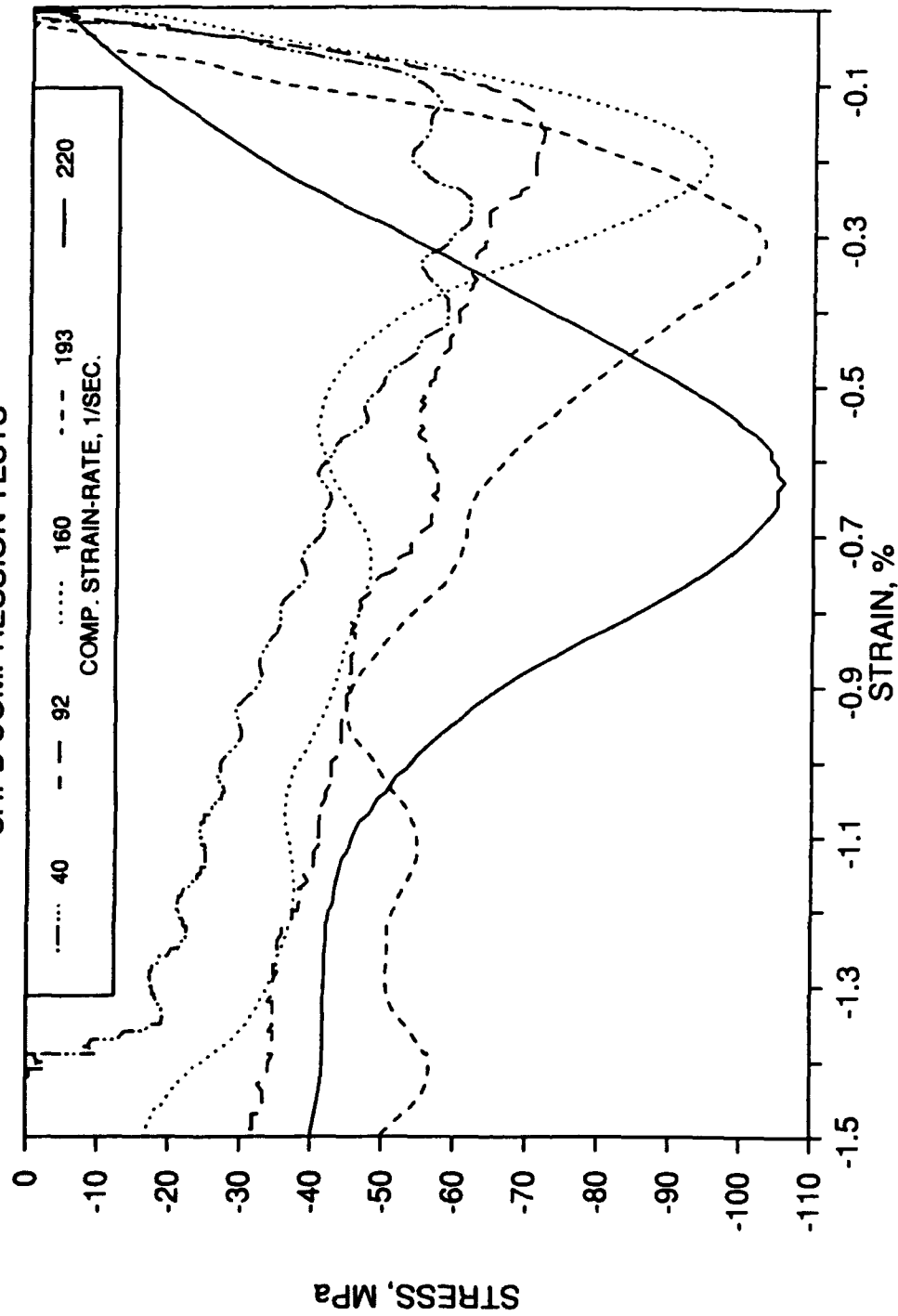


Figure 10. Strain-Rate Effects on the Shape of the Stress-Strain Curve.

STRAIN AT PEAK STRESS VS STRAIN-RATE SHPB CONCRETE TESTS, $f'_c = 48.3$ MPa

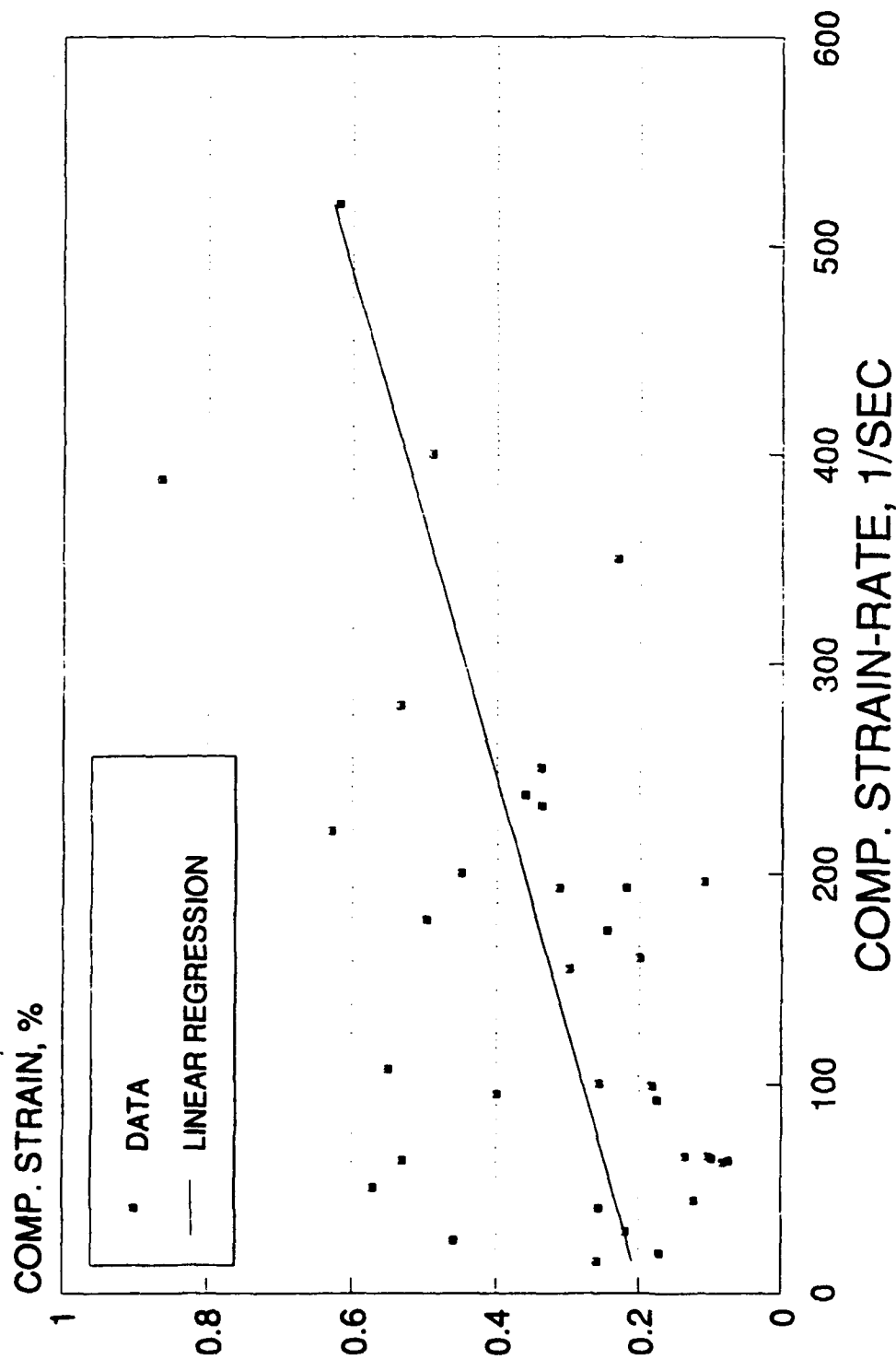


Figure 11. Strain-Rate Effects on the Strain at Peak Stress.

STRAIN RATE EFFECTS ON CONCRETE STRENGTH

TENSION TESTS

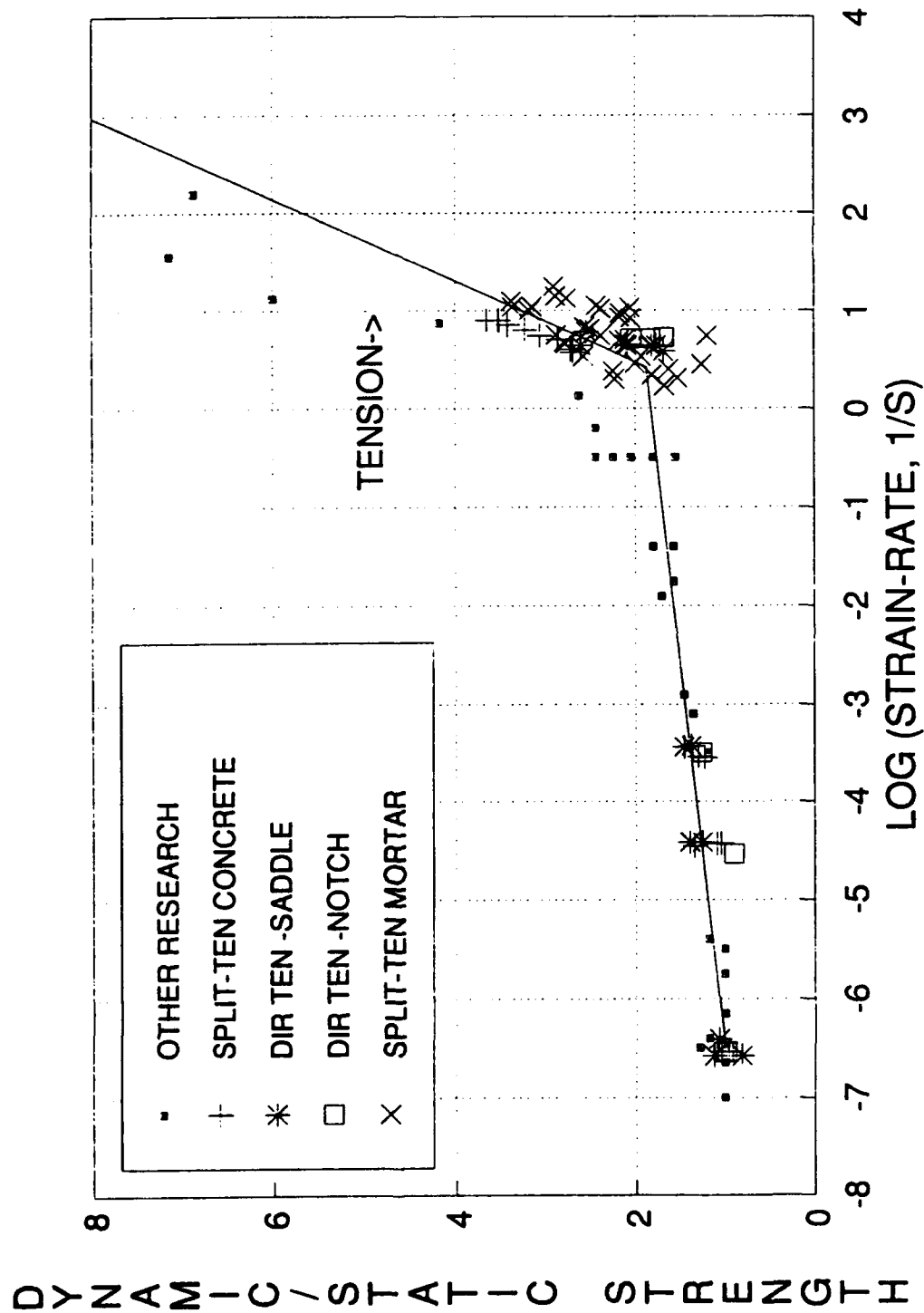


Figure 12. Tensile Concrete Data Obtained Using the RACS/AFCEA SHPB.

of the compressive curve. In observing the tensile stress-strain curves of concrete it appears the initial slope does not change and that both the peak stress and associated strain change by the extension along this initial slope. It is further assumed that the initial static slope (Young's modulus) does not change with strain rate.

B. CRACK INITIATION AND DENSITY

1. Crack Initiation

Compressive concrete specimens were instrumented as shown in Figure 3 and placed in the SHPB as shown in Figure 5. Eight instrumented specimens were tested at eight different strain rates. Instrumented compression specimens were tested in the SHPB at preselected gas gun pressures which produce a measurable strain rate. Simultaneous recording of the incident strain pulse, reflected strain pulse, transmitted strain pulse, twelve break circuits, camera and four specimen strain gages is controlled by the oscilloscope and delay generator. The strain pulses are recorded on the oscilloscope, the break circuits and specimen strain gages are recorded on the TDR and the crack pattern is recorded on the camera film sheet.

Crack initiation is determined from the break circuit (BC) traces by recording the jump in voltage for each BC. Examples of the recorded BC traces are given in Figures 13, 14 and 15 for the specimen DCI-2. Strain gage (SG) traces for this same specimen are given in Figure 16. Both the BC traces and SG traces were transferred from the TDR to LOTUS® and Freelance® programs for plotting in final form.

INSTRUMENTED DIRECT COMPRESSION

SPECIMEN DCI-2

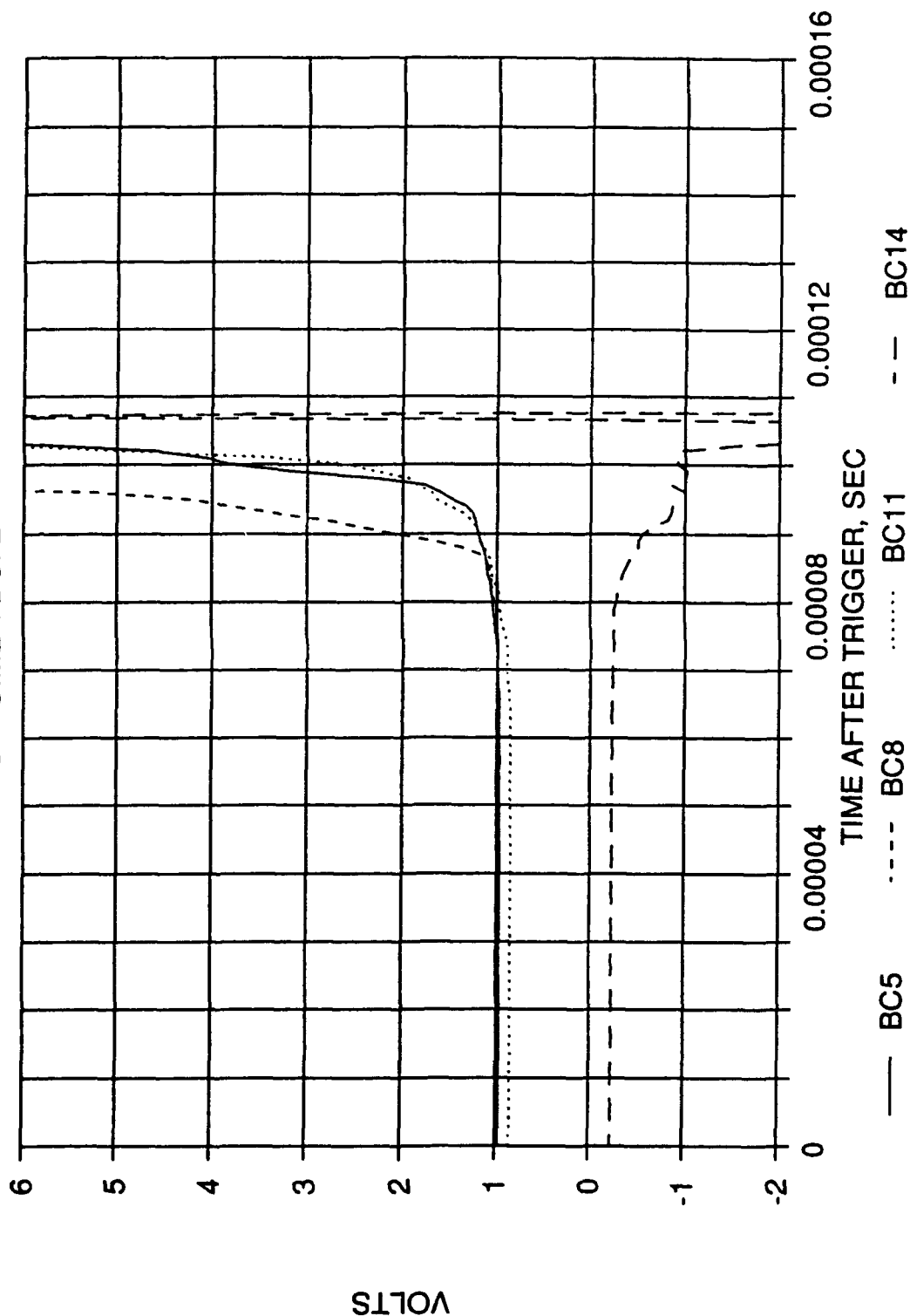


Figure 13. Break Circuits Traces for the Array on the Incident End of the Specimen (Array A of Figure 3, Specimen DCI-2, Strain Rate = 92/sec).

INSTRUMENTED DIRECT COMPRESSION

SPECIMEN DCI-2

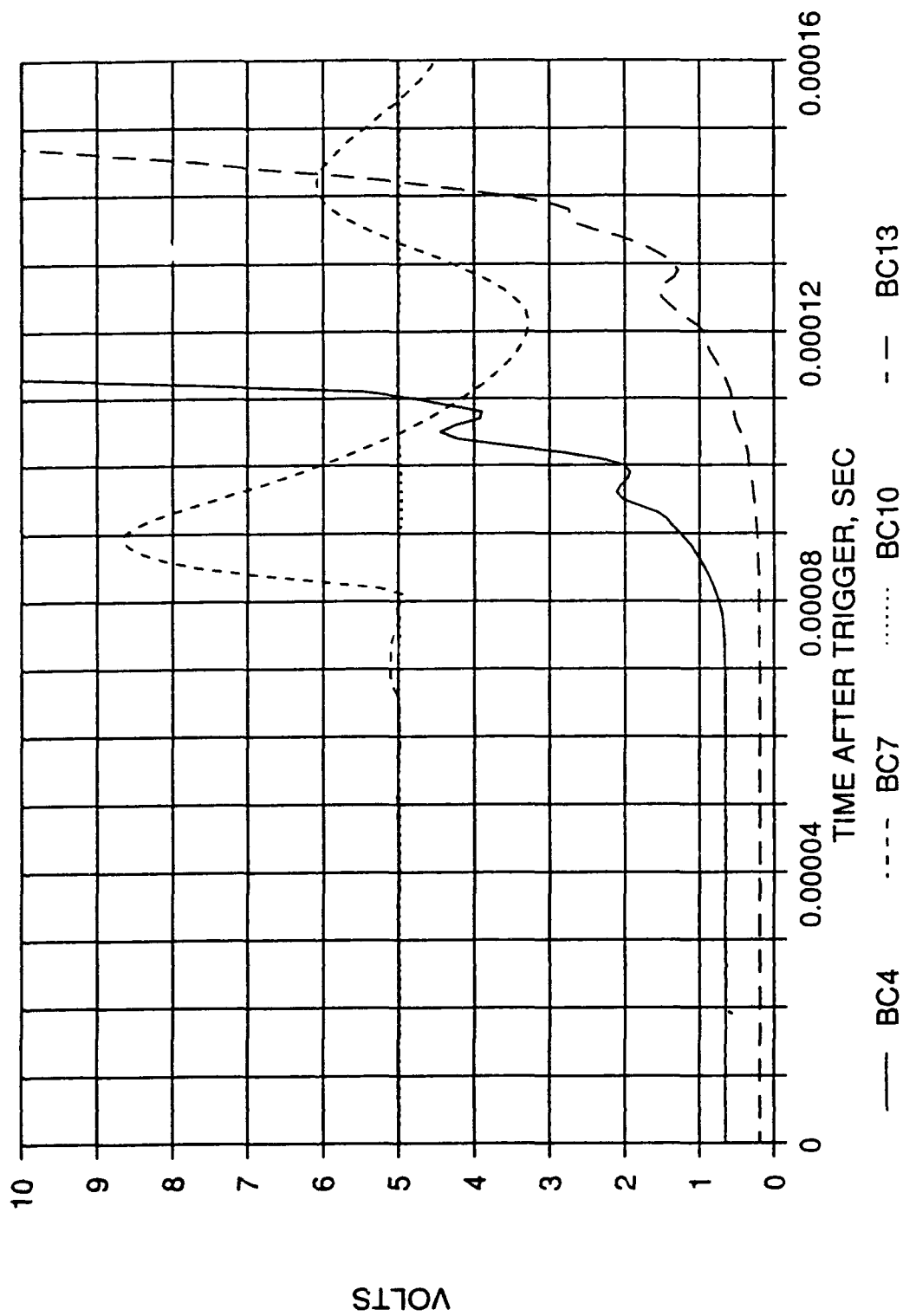


Figure 14. Break Circuits Traces for the Array at Midsection of the Specimen (Array B of Figure 3, Specimen DCI-2, B Strain Rate = 92/sec).

INSTRUMENTED DIRECT COMPRESSION

SPECIMEN DCI-2

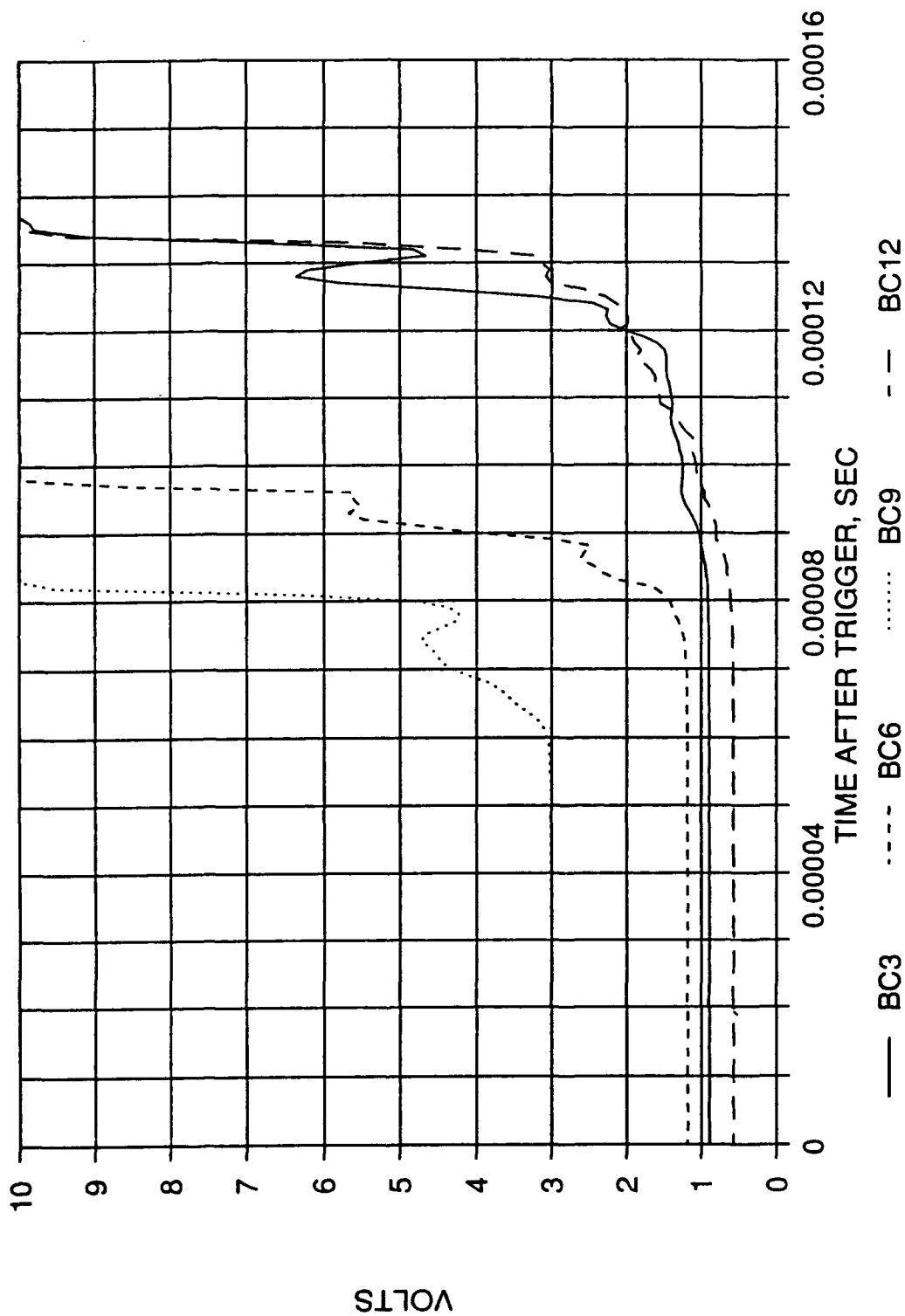


Figure 15. Break Circuit Traces for the Array on the Transmitter End of the Specimen (Array C of Figure 3, Specimen DCI-2, Strain Rate = 92/sec).

INSTRUMENTED DIRECT COMPRESSION

SPECIMEN DCI-2

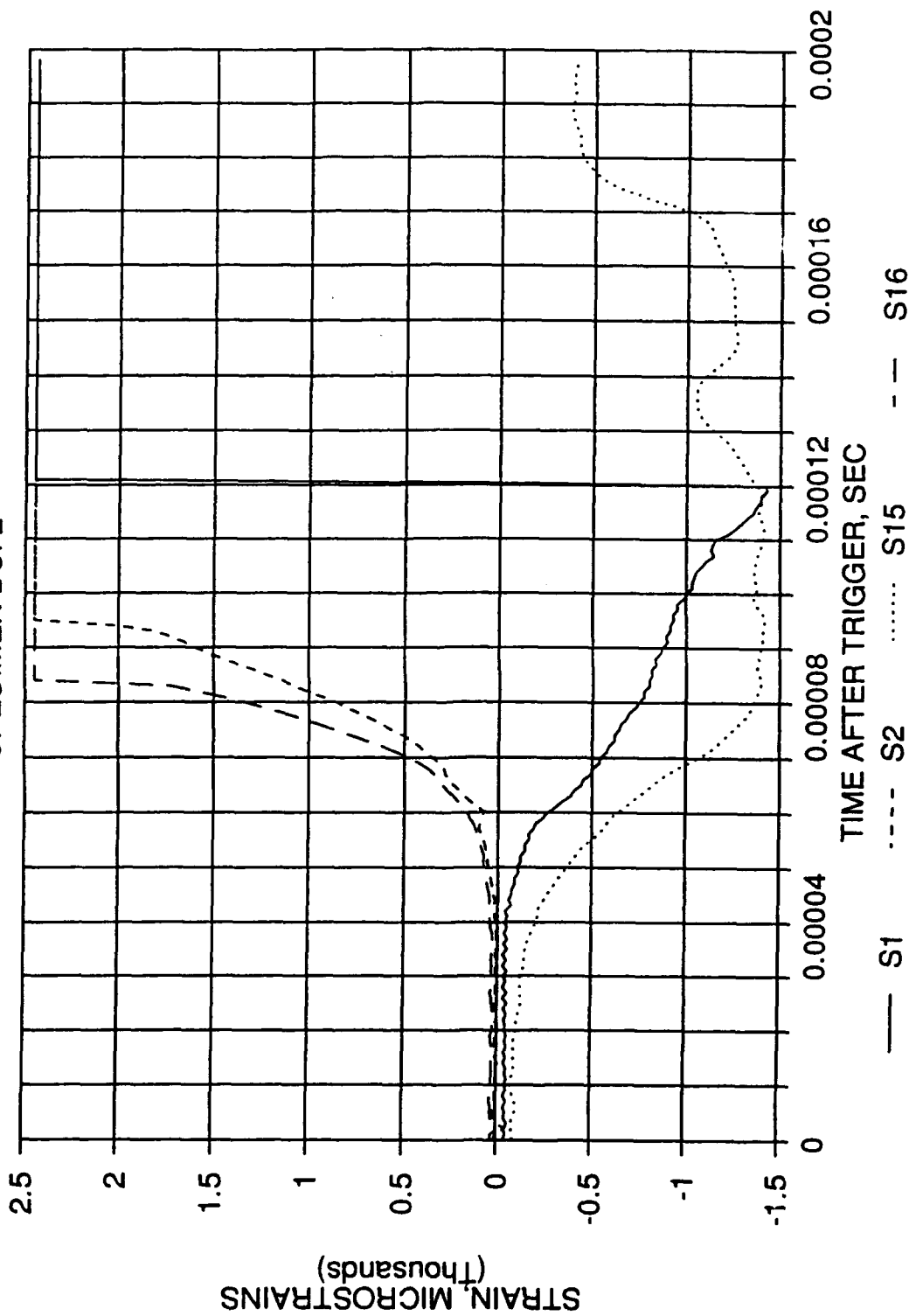


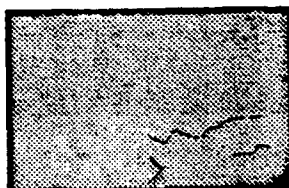
Figure 16. Strain Gage Traces for Specimen DCI-2, Strain Rate - 92/sec.

2. Crack Density

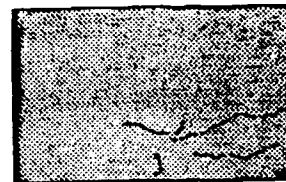
An image of the crack pattern forming on the specimen surface was recorded on Polaroid film (Figure 6) but these images are difficult to copy and some enhancement is required. This enhancement process is straight forward but time consuming. Each frame of the Polaroid film is enlarged and frozen on the monitor screen of the Omninet II®. With the frame frozen on the screen the original picture may be picked up and examined closely for the cracks. Using both the screen image and the original picture the cracked pattern is "painted" electronically using a one pixel wide black line. The one-pixel wide line allows for calibration of crack length. Since the "painted" line is one pixel wide, when an area measurement is made the area becomes the line length. Calibration is made by "painting" a black line across the 2 inch (50.8 mm) long specimen in the picture and the area measurement, indicated by an area measurement command of the computer, becomes a 2 inch (50.88 mm) long line of the specimen. This area measurement or crack length is made and recorded for each frame.

After each frame is analyzed for crack length it is stored as a grey file. Each grey file must then be down loaded to a floppy disk which is displayed on an IBM® PC using a locally generated program. Each frame or image is then sized, annotated and stored for printing using Word Perfect® software. The final display of crack patterns for three different specimens at three different strain rates are shown in Figures 17 to 19.

Times for all events were synchronized relative to the trigger time of the TDR and the ultra-high-speed camera. This means that each frame of the crack patterns may be related to specimen strain as shown in Figure 20. Then for each crack pattern there is a given strain, strain rate and total crack length from image analysis, all given for the same time. The total crack



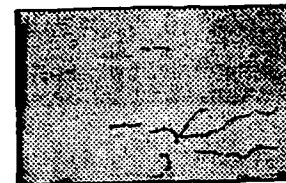
DCI-9-3



DCI-9-4



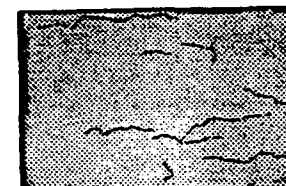
DCI-9-5



DCI-9-6



DCI-9-7



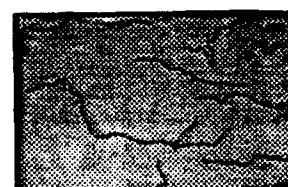
DCI-9-8



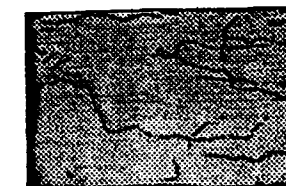
DCI-9-9



DCI-9-10



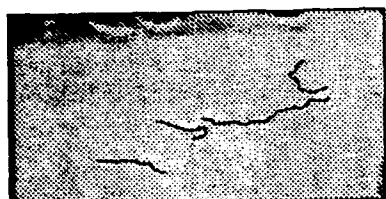
DCI-9-11



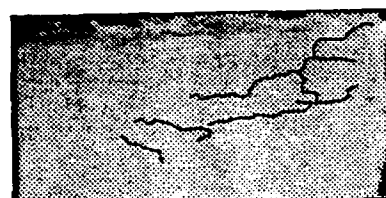
DCI-9-12

10 μ sec between frames, Strain-rate 65/sec

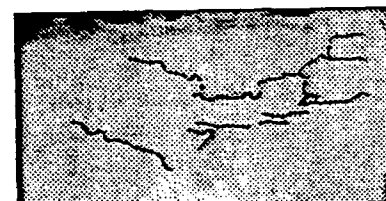
Figure 17. Crack Patterns for Deforming Specimen DCI-2, Strain Rate = 92/sec.
Ten Microseconds between Frames.



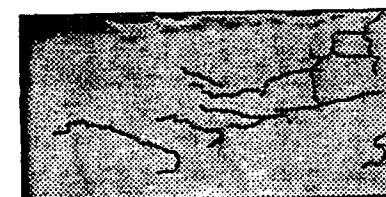
DCI-2-5



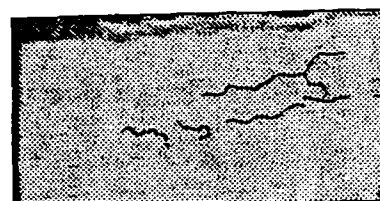
DCI-2-7



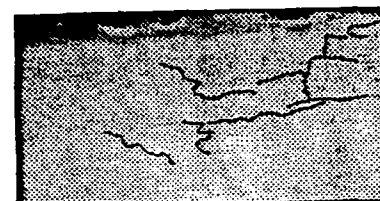
DCI-2-9



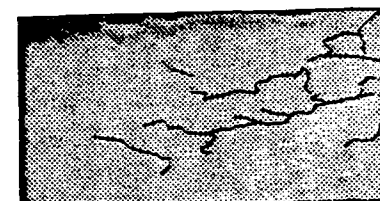
DCI-2-11



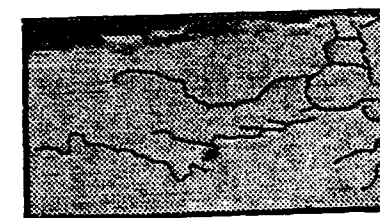
DCI-2-6



DCI-2-8

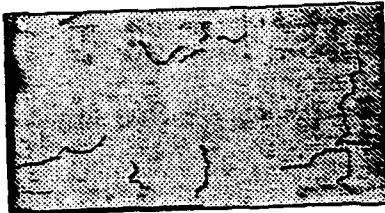


DCI-2-10



DCI-2-12

Figure 18. Crack Patterns for Deforming Specimen DCI-9, Strain Rate = 65/sec.
Ten Microseconds between Frames.



DCI-8-5



DCI-8-6



DCI-8-7



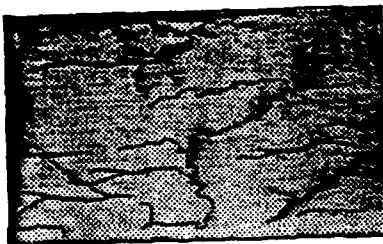
DCI-8-8



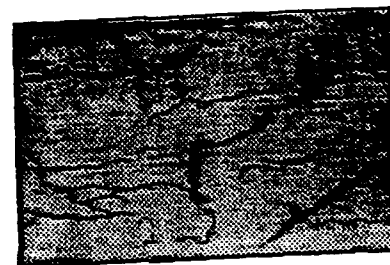
DCI-8-9



DCI-8-10



DCI-8-11



DCI-8-12



DCI-8-13



DCI-8-14

Figure 19. Crack Patterns for Deforming Spceimen DCI-8, Strain Rate = 220/sec
Ten Microseconds between Frames.

INSTRUMENTED DIRECT COMPRESSION

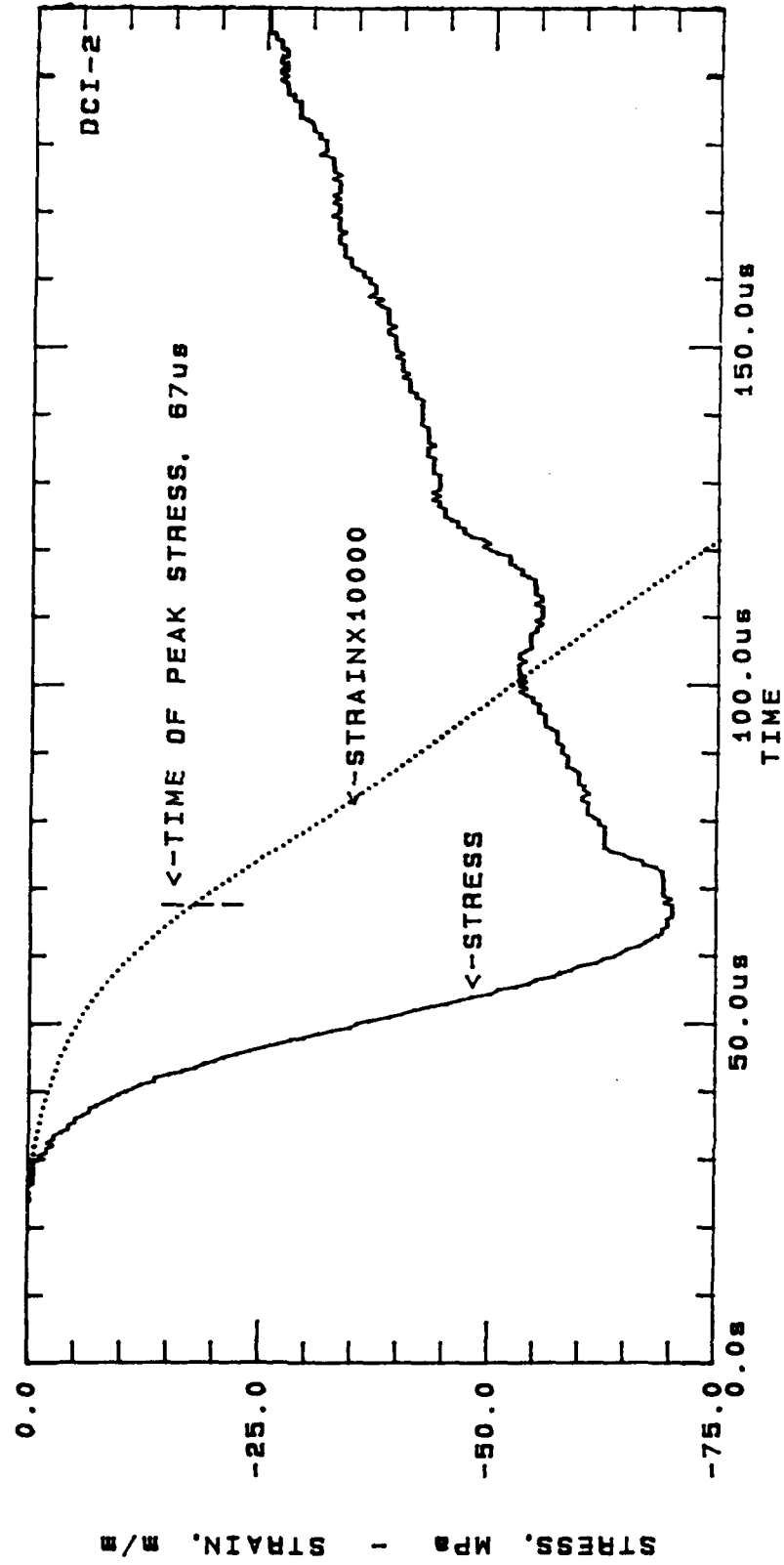


Figure 20. Stress and Strain Versus Time after Trigger for Specimen DCI-2. This Data Obtained from SHPB Traces.

CRACK SURFACE DISTRIBUTION

SHPB CONCRETE TESTS, $f'_c = 48.3$ MPa

SR = COMP. STRAIN-RATE, 1/SEC

| | | | | | | | |
|---|----------|---|----------|----|----------|---|----------|
| ◇ | SR = 220 | × | SR = 160 | () | SR = 92 | * | SR = 65 |
| + | SR = 62 | • | SR = 95 | △ | SR = 200 | × | SR = 107 |

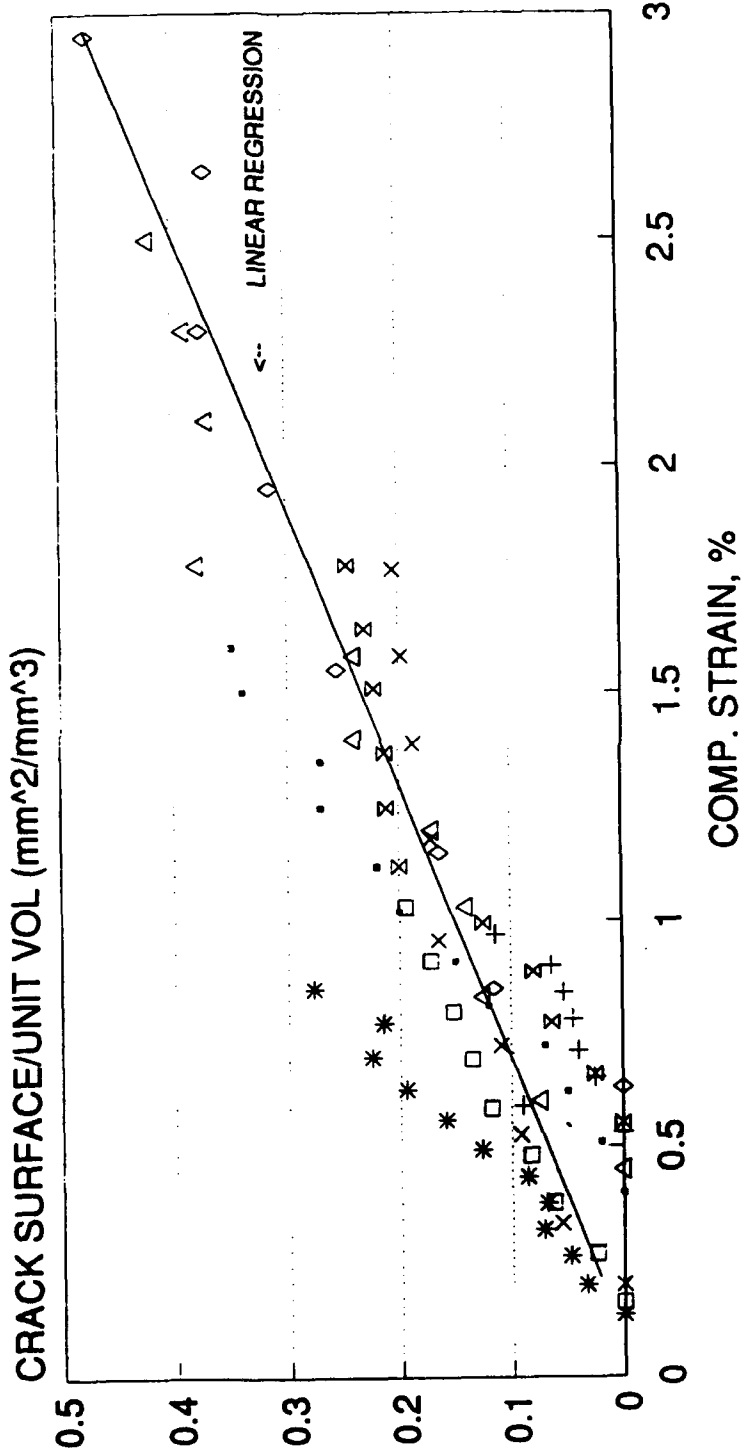


Figure 21. Crack Surface/Volume versus Compressive Axial Strain for Different Strain Rates.

CRACK SURFACE DISTRIBUTION/VOLUME

SHPB CONCRETE TESTS, $f'_c = 48.3$ MPa

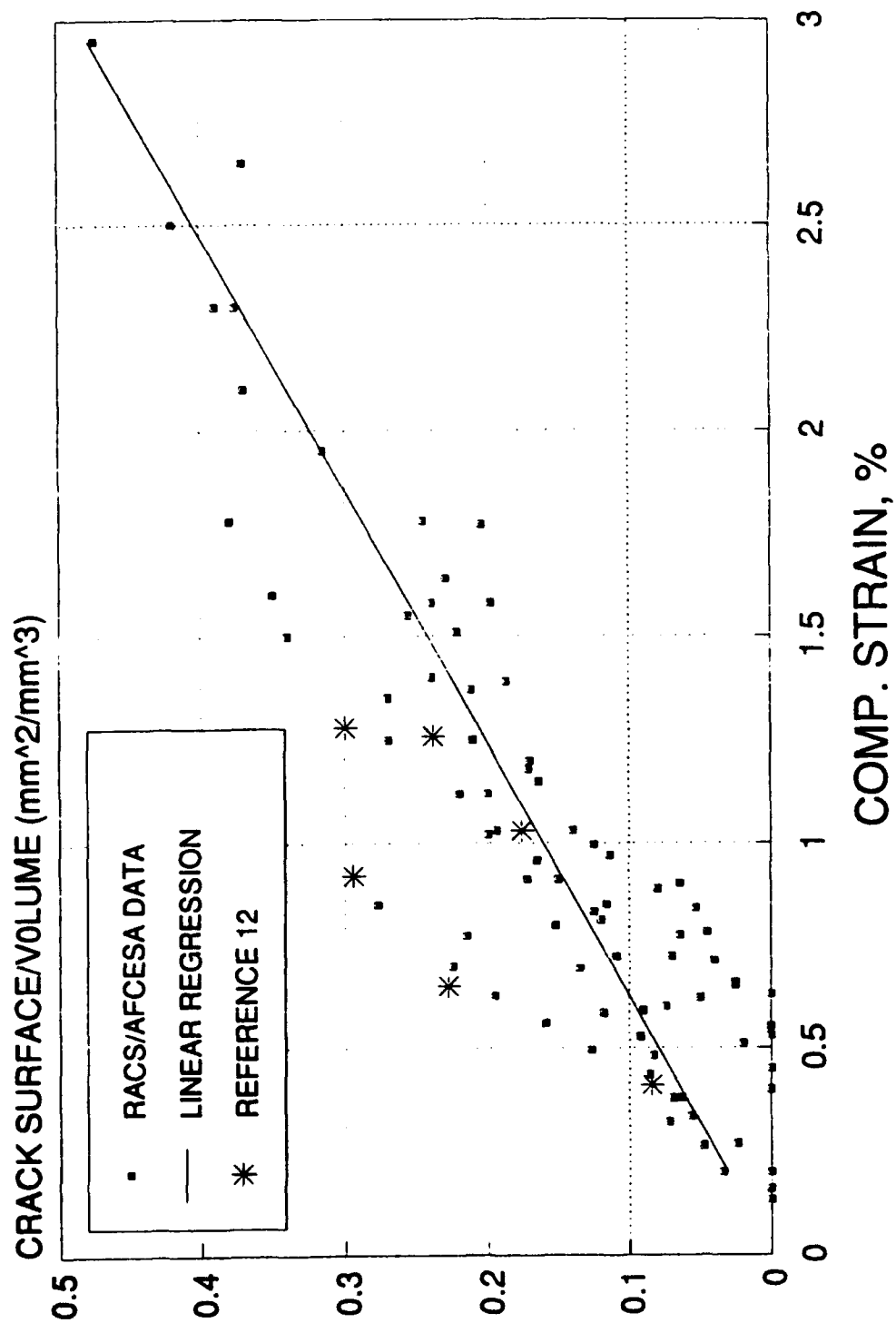


Figure 22. All Crack Surface/Volume Data Excluding Initial Strains Used in Linear Regression.

INSTRUMENTED DIRECT COMPRESSION

SPECIMEN DCI-2

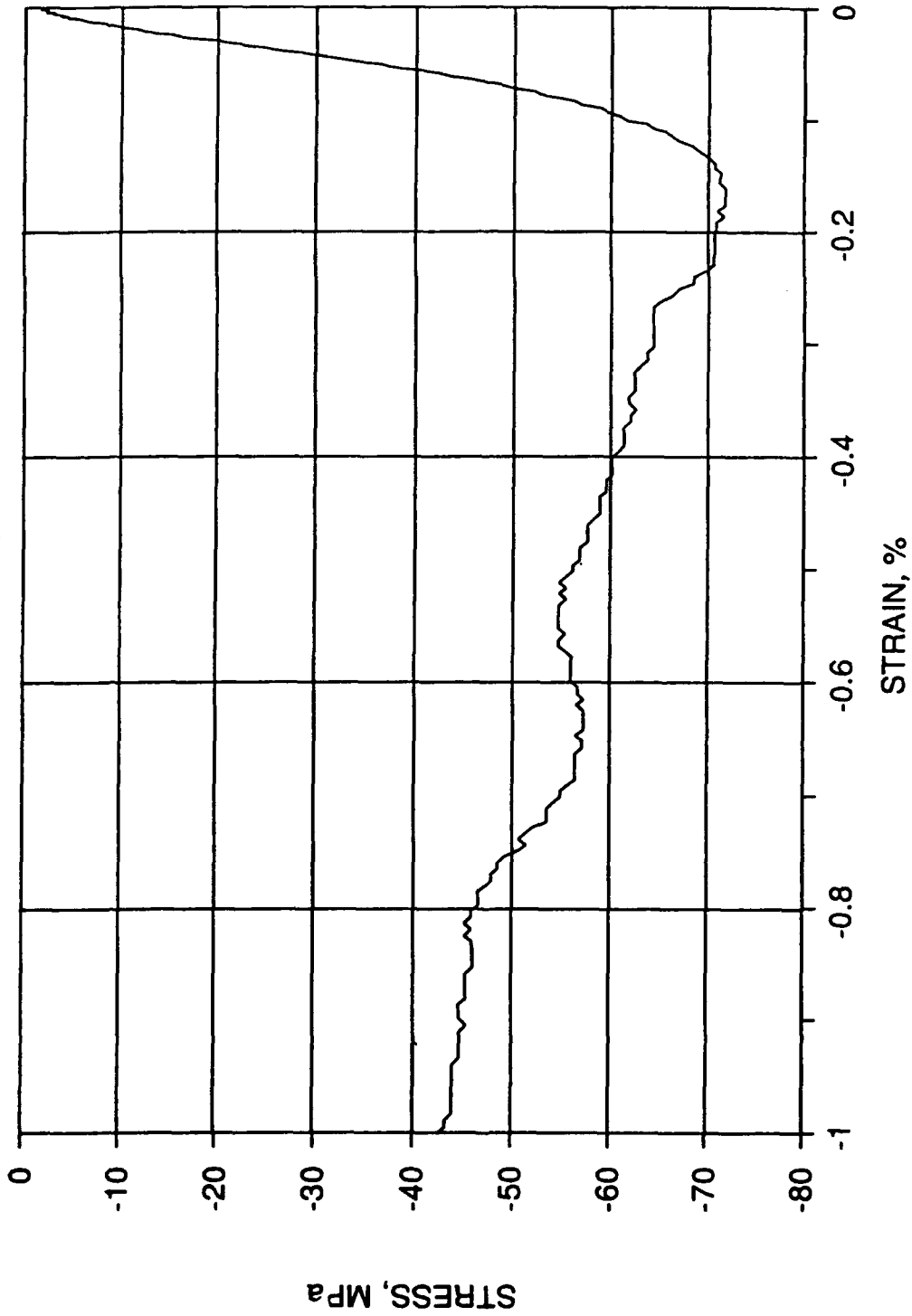


Figure 23. Stress-Strain Curve for Specimen DCI-2, Strain Rate = 92/sec. Range of Strain 0.0 to 1.0%.

INSTRUMENTED DIRECT COMPRESSION

SPECIMEN DCI-2

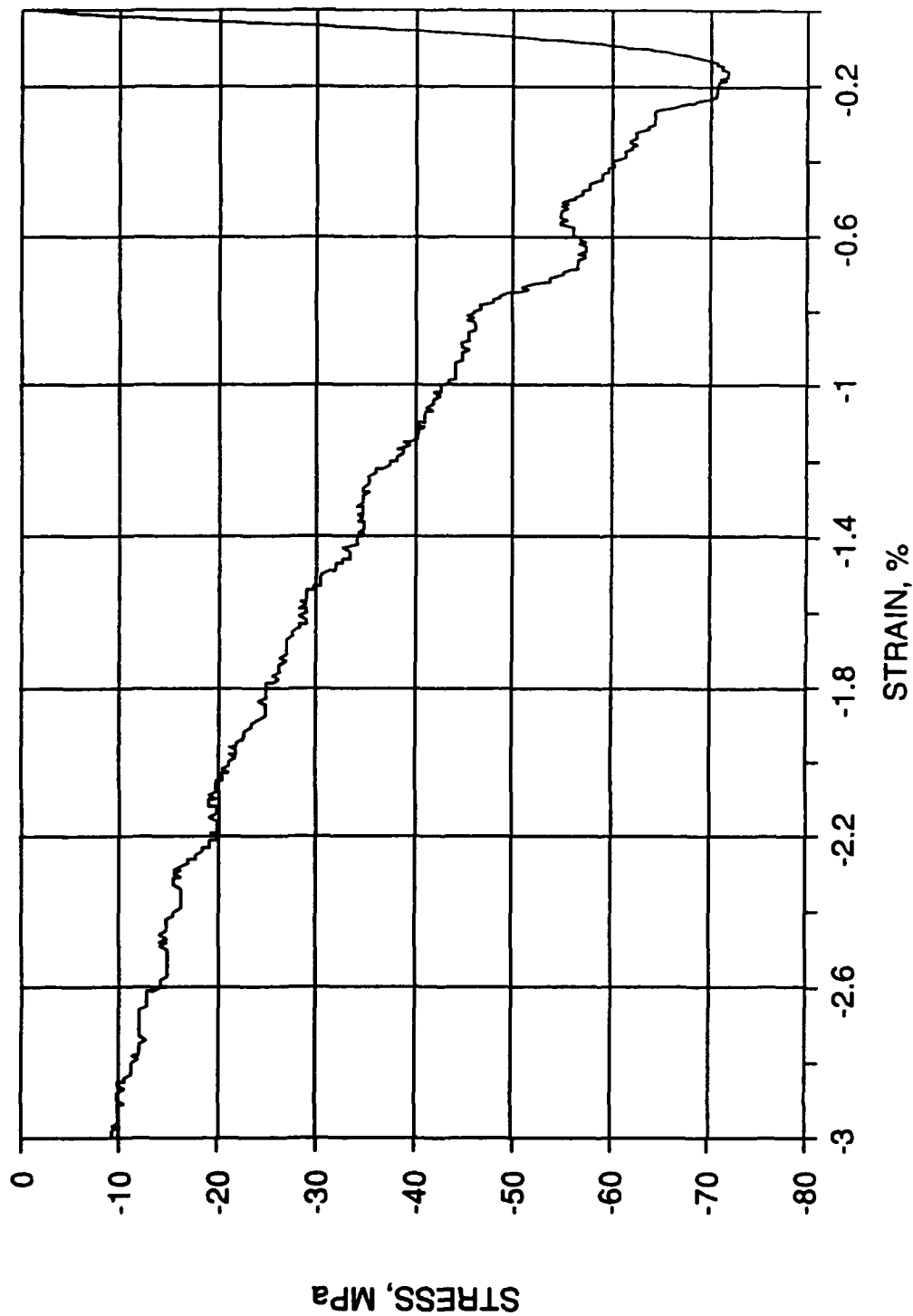


Figure 24. Stress-Strain Curve for Specimen DCI-2, Strain Rate - 92/sec. Range of Strain 0.0 to 3.0%.

length for each frame is converted to length/surface by dividing by the area of the 60° arc of surface for a 2.0 inch (50.8 mm) long specimen. Further assuming that the crack pattern is random the crack length/surface may be converted to crack surface/volume by multiplying by $4/\pi$ (Reference 11). The experimental crack density results of eight different specimens at eight different strain rates are shown in Figure 21. A linear regression for all the data of Figure 21 excluding the initial strains (strains on the abscissa) was performed and shown in Figure 22.

C. DISCUSSION

1. Crack Initiation and Strain Data

In all the experimental observations on SHPB, direct compression of concrete made using the ultra-high-speed camera, the first cracks appear at the peak load or stress. However, there is an error of approximately ten microseconds, the time between frames of the film. Comparing the data from the SHPB, TDR and camera for one specimen it is surprising how well they correlate. Figures 23 and 24 show a stress-strain curve for Specimen DCI-2 with a peak stress of -70.2 MPa and strain at peak stress of -1670 microstrains at a time of 67 microseconds taken from Figure 20. In comparison the compressive strain on the specimen (Figure 16) is approximately -1400 microstrains. The break circuits of Figures 13-15 show a change in voltage at approximately 75 microseconds. For the photograph and the enhanced version of Figure 17 the initial cracks form between the frames of 75 microseconds and 85 microseconds. With a variation of ± 5 -10 microseconds all the recorded events occur at approximately the same time. This leads one to conclude that peak stress and the visible macrocracks occur at about the same time and at a transverse tensile strain of 500 to 1000 microstrains. This tensile strain is an estimate of the critical

dynamic tensile strain at tensile strain rates of 1 to 20/seconds. The critical static-tensile strain (onset of visible cracks and at peak stress) is on the order of 100 microstrains for concrete. The other conclusion gleaned from this data is that the cylindrical concrete specimen fails initially by longitudinal cracks initiated by transverse tensile strain which results from a Poisson effect since there is no applied transverse tensile stress. The average of the transverse to axial strain ratio of the two sets of strain gages of one specimen is shown in Figure 25. This figure is not as smooth as one would like but remember we are dealing with an event lasting only a few microseconds. The general observation here is that the strain ratio is close to -0.22 , equivalent to a Poisson ratio of 0.22 , up to 50 to 60 microseconds and after that it decreases drastically and is approximately -1.0 at the peak stress. Near the 50 to 60 microsecond points of the strain ratio (Figure 24) corresponds to 50 to 75 percent of the peak stress of Figure 20. This percentage of peak stress in a static concrete compression corresponds to the beginning of nonlinear or plastic behavior.

2. Crack Density and Damage Model

In this section reference is made to both a crack density defined as crack surface per unit volume and a crack density parameter which is non-dimensional but represents the damaged volume per volume of original material. The crack density is the experimentally determined crack length/unit area multiplied by the $4/\pi$ factor, which converts the crack density to a crack surface per unit volume. A linear regression was calculated, and shown in Figure 22, which gives a crack density of 0.5 at a strain of approximately 3.0%. Data from Reference (12) is also shown in Figure 22. However, the Reference (12) data was obtained by limiting the strain in a SHPB by a collar slightly shorter than the specimen, removing the specimen intact, placing it in a crack

TRANSVERSE/AXIAL STRAIN RATIO

CONCRETE SPECIMEN DCI-2

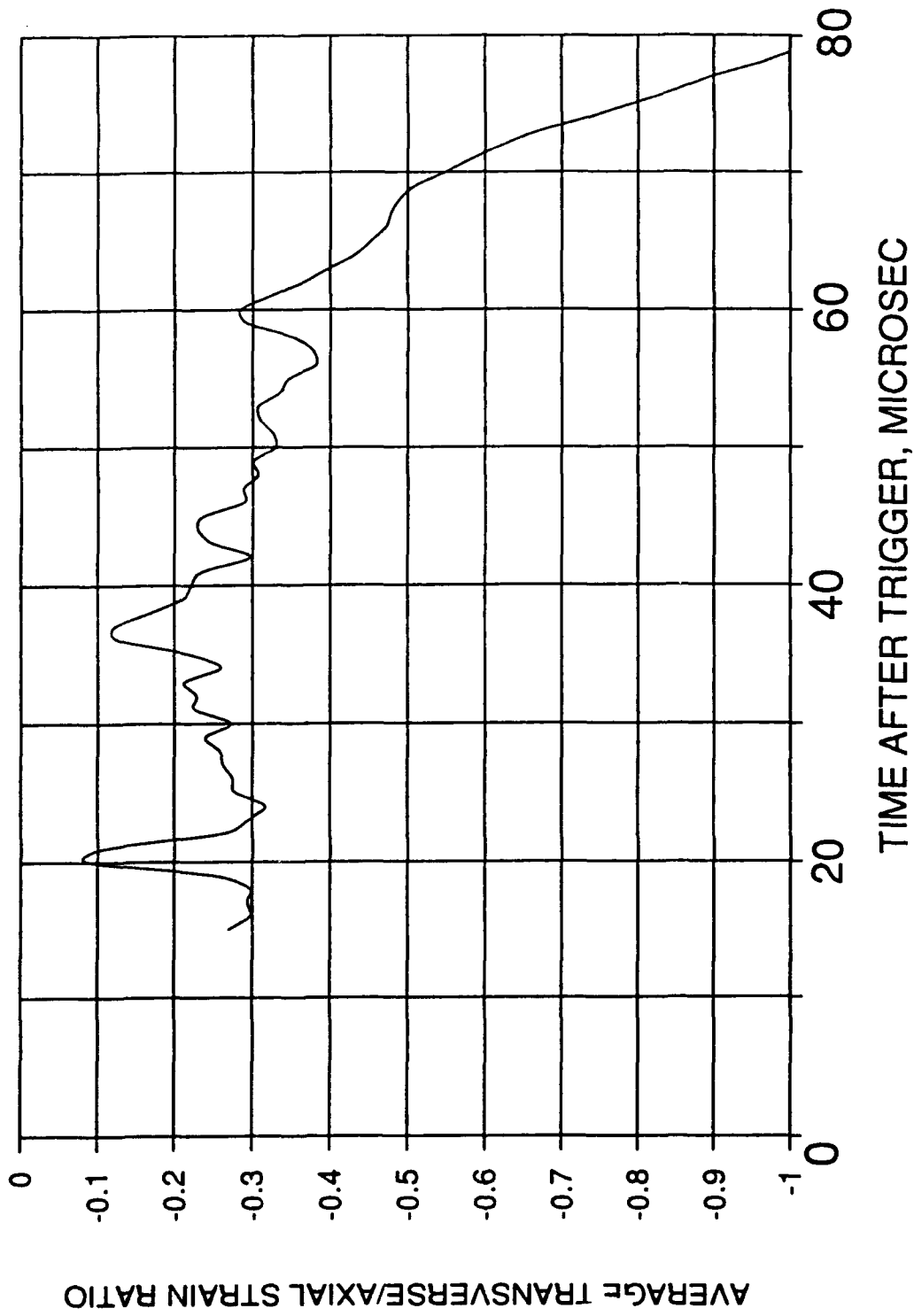


Figure 25. Transverse Axial Strain Ratio for Specimen DCI-2, Strain-Rate - 92/sec.

enhancing epoxy solution, sectioning the specimen and observing the crack pattern. In comparison the data obtained in this study is considered to be real time data recorded during the actual event. That the work in Reference (12) was accomplished at the University of Florida¹ and is being continued under partial sponsorship by RACS/AFCEA through AFOSR.

Based on methods presented in Reference (8) the upper limit of the crack density parameter is $9/16$ (0.5625) but is a dimensionless parameter. How one would convert the crack density of Figure 22, which is a crack surface/volume (mm^2/mm^3), to the nondimensional crack density parameter is debateable, to say the least. However, in observing the stress-strain curves such as Figure 24 the strength has been reduced to approximately 10% or less of the maximum strength at 3.0% strain. Using the regression curve of Figure 21 or 22 gives a linear expression of crack density C_d relative to compressive axial strain ϵ_c as

$$\bar{C}_d = 16.12\epsilon_c \quad (10)$$

where \bar{C}_d has units of mm^2/mm^3 and ϵ_c had units of mm/mm . Using Equation (10) and a $\bar{C}_d = 9/16$ gives a strain of 3.5%. If we assume that the cracks at specimen surface have reached an opening or width of 1.0 mm will convert the crack density to the crack density parameter C_d . This means that at approximately 3.5% axial compressive strain the load carrying ability has been reduced to zero, C_d has locally reached its maximum, from Equation (9) the damaged Poisson's ratio goes to zero, from Equation (7) the damage parameter D goes to unity and the damage bulk modulus \bar{K} goes to zero. In other words, the material can no longer resist any load.

The above discussion is based on a uniaxial high-strain-rate test on a small 50.8 mm long small aggregate concrete cylinder.

¹Malvern, L. E. and Jenkins, D. A., Dept. of Aero., Eng. Mech. & Sci., University of Florida, Gainesville, FL 32611

Further assumptions of linearity of strain at peak stress or strength could lead to an expression of \bar{C}_d as a function of strain and strain rate. Since the strain at peak stress is a function of strain rate then crack initiation strain for a given strain rate is variable along the $\bar{C}_d = 0$ axis (abscissa) of Figure 21. This means that a curve of \bar{C}_d versus strain for a given strain rate would start at a point on the abscissa or $\bar{C}_d = 0$ line and curve upward becoming asymptotic to the regression line of Figure 21. A hyperbola with the transverse axis parallel to the abscissa of Figure 21 would lend itself to this description but is not pursued here due to the limited amount of data on the relation of strain at peak stress to strain rate.

SECTION V
CONCLUSIONS AND RECOMMENDATIONS

The small concrete specimens used in the SHPB strength tests appear to fail by longitudinal macrocracking at the time of the peak load. This was verified by a series of break circuits and the ultra-high-speed camera recording.

As the strain rate increases both the strength (peak stress) and critical strain associated with this peak stress increases. The total crack length/unit surface area of the specimen starts at the peak stress or critical strain, rises sharply and then follows a linear function of strain up to a complete loss of load-carrying capacity. Using the experimentally determined crack density a damage parameter and associated damage modulus may be calculated.

Continued study is recommended to better describe the crack density parameter but a better image analysis technique is needed. Further SHPB tests on small concrete specimens are recommended to better describe the strain at peak stress.

REFERENCES

1. Malvern, L. E., Tang, T., Jenkins, D. A., and Gong, J. C., "Dynamic Compressive Strength of Cementitious Materials," Material Research Society, Symposium Proceedings, Vol. 64, pp. 119-138, 1986.
2. Ross, C. A., Split-Hopkinson Pressure Bar Tests, ESL-TR-88-22, Engineering and Services Laboratory, Air Force Engineering and Services Center, Tyndall AFB, Florida, March 1989.
3. Reinhardt, h. W., "Tensile Fracture of Concrete at High Rates of Loading," in Application of Fracture Mechanics to Cementitious Composites, ed., S. P. Shah, Martrius Nijhoff Publishers, Boston, pp. 559-590.
4. Gopalaratnam, V. S., Shah, S. P. and John, R. "A Modified Instrumented Charpy Test for Cement Based Composites," Experimental Mechanics, June 1984, pp. 102-111.
5. Malvern, L. E., Jenkins, D. A., Jerome, E., and Gong, J. C., Dispersion Correction for Split-Hopkinson Pressure Bar Data, ESL- TR-88-ODC Engineering & Services Laboratory, AF Engineering & Services Center, Tyndall AFB, Florida, 32403, July 1988.
6. Krajcinovic, D. "Continuum Damage Mechanics," Appl. Mech. Rev. 37(1), 1984, pp. 1-6.
7. Budiansky, B. and O'Connell, R. J. "Elastic Moduli of a Cracked Solid," J. Solids and Structures, 12, 1976, pp. 81-97.
8. Taylor, L. M., Chen, En-P., and Kuszmaul, J. S., "Microcrack-Induced Damage Accumulation in Brittle Rock Under Dynamic Loading," Computer Methods in Applied Mechanics and Engineering, 55, 1986, pp. 301-320.
9. Malvern, L. E. and Ross, C. A., Dynamic Response of Concrete and Concrete Structures, Two annual reports and a final report for AFOSR Contract F49620-83-D007. University of Florida, Gainesville, FL, 1984, Feb. 1985, May 1985.
10. Malvern, L. E. and Jenkins, D. A., Dynamic Testing of Laterally Confined Concrete, ESL-TR-89-47, Engineering and Services

Laboratory, Air Force Engineering and Services Center, Tyndall A.F.B., FL. 1990.

11. Underwood, E. E., "Surface Area and Length in Volume," Quantitative Microscopy, eds. Dekoff, R. T. and Rhine, F. N., McGraw-Hill, New York, 1968, pp. 78-125.
12. Malvern, L. E., Jenking, D. A., Tang, T. and Gong, J-C. "Dynamic Testing of Concrete with Split Hopkinson Pressure Bar," Proceedings Fourth International Symposium on the Interaction of Non-Nuclear Munitions with Structures (Vol. 1), Panama City Beach, FL, April 1989, pp. 296-299.